Chapter 3

Development of Amorphous Silicon Alloy Thin Film Light Emitting Diode
with a-SiN:H as a Luminescent Layer

3.1 Introduction

The interesting wide optical energy gap amorphous silicon alloys studied in this thesis are a-SiN:H, a-SiC:H and a-SiO:H. This chapter will start with the a-SiN:H and its application to the thin film LED (TFLED).

The hydrogenated amorphous silicon nitride (a-SiN:H) alloy has been widely studied by many research groups from the viewpoint of both basic properties and possibility of application to electronic devices [1-11]. The main applications of a-SiN:H up to date , such as a passivation layer on an electronic device and a gate layer in a thin film transistor (TFT) have been focused on its excellent insulating properties. Concerning its semiconducting properties, there were some reports on the optical properties of a-SiN:H [12]. They reported that visible photoluminescence was able to be observed in the a-SiN:H which has an optical energy gap larger than about 2.2 eV. However, there has been no report on the application of a-SiN:H as a luminescent active layer in any light emitting device so far.

Amorphous silicon nitride was generally prepared by a glow discharge plasma CVD method from a mixture of silane and either ammonia or nitrogen. In this thesis, ammonia was used as the gas source. It is generally found that increasing nitrogen content the optical energy gap of the film will increase from 1.7 eV to about 5 eV.

In this chapter, the preparation, basic structural and optical properties of a-SiN:H materials are described. The focus will be placed on the photoluminescent properties of undoped a-SiN:H. A series of experiments has been made to develop an injection type electroluminescent device with the p-i-n junctions where the i-layer is made of undoped a-SiN:H. Some technical data on the device fabrication technologies, device structure, LED characteristics and carrier injection mechanism

are presented. The discussion will be done on the connection between the carrier injection mechanism and electroluminescent characteristics. A particular emphasis has been placed on the dependence of these characteristics on the material properties and the thickness of the i-a-SiN:H layer [13-17].

3.2 Structural properties of a-SiN:H film

3.2.1 Measurement of Hydrogen Contents in a-SiN:H Film by Infrared Absorption Spectra

Amorphous silicon nitride (a-SiN:H) thin films were prepared by the glow discharge plasma CVD system as mentioned in chapter 2. The typical preparation conditions for undoped a-SiN:H are summarized in Table 3.1

Table 3.1 Typical preparation conditions for undoped a-SiN:H.

RF power	4 watt (13.56 MHz)
Substrate temperature	190 °C
Pressure	1.0 Torr
SiH_4 gas flow	30 - 70 cc/min
NH_3 gas flow	30 - 70 cc/min
Film thickness	1.0 - 1.5 micron

High resistivity, single-crystalline Si wafers were used as the substrates for IR absorption measurements. Float-zone-growth wafers were preferred because of their low oxygen contents, although the more widely-available Czochralski-grown Si wafers were acceptable for dual-beam measurements. The thickness of the substrates was about 400 micron. The size of the substrate was about 1.0 x 1.0 cm^2.

Figure 3.1 shows an example of the room temperature infrared transmittance spectrum for undoped a-SiN:H film prepared at $NH_3/(SiH_4 + NH_3)$ gas ratio x = 0.71. The absorption peaks are observed at around the 850 1/cm due to Si-N asymmetric stretching vibration mode, and at around 2100 1/cm and 3350 1/cm due to Si-H stretching and N-H stretching modes, respectively. Figure 3.2 shows the contents of
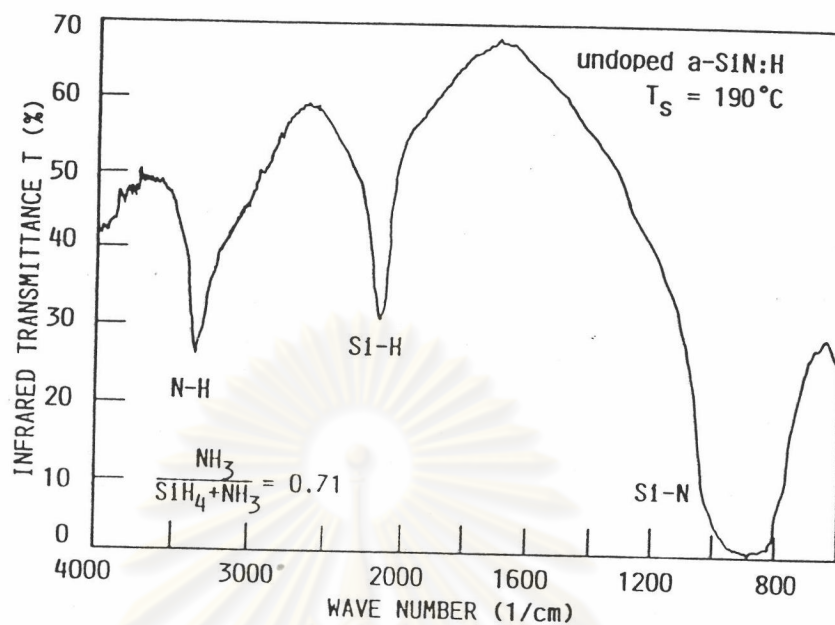
Figure 3.1 Infrared transmittance spectrum for a-SiN:H film prepared at NH_3 / (SiH_4 + NH_3) ratio x = 0.71.
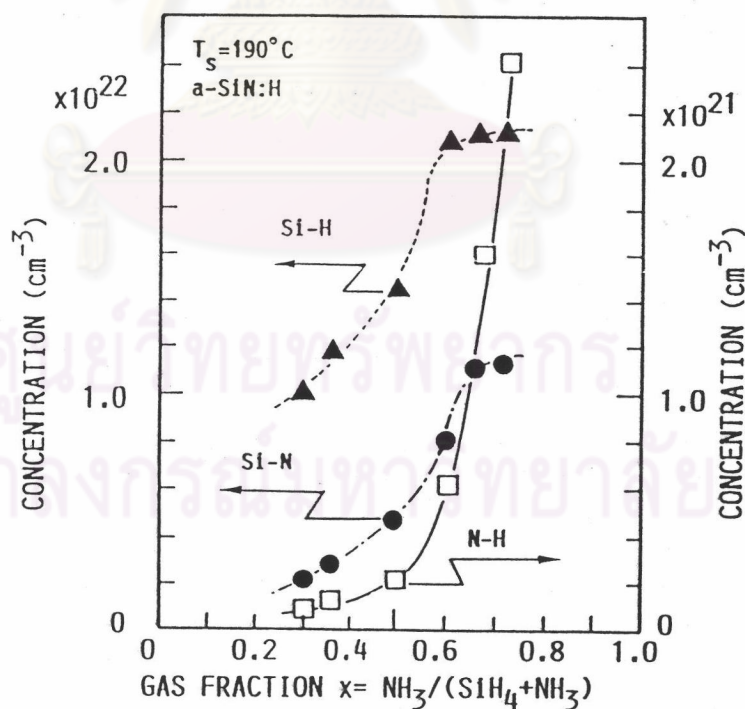

Figure 3.2 Contents of Si-H bonds derived from stretching and wagging modes and content of N-H bonds derived from stretching mode as a function of the ammonia gas fraction x.

Si-H bonds derived from stretching and wagging modes and content of N-H bonds derived from stretching mode as a function of the ammonia gas fraction x. The content of the H-bonded with N (N_{N-H} ($1/cm^3$)) was calculated from the formula :

$$N_{N-H} \quad = \quad A \int \frac{\alpha(\omega)}{\omega_0} \tag{3.1}$$

where A: proportionality constant, here $A = 2.8 \times 10^{20}$ $1/cm^2$ for N-H bonds [18].

α: absorption coefficient,

ω: wave number,

and ω_0: wavenumber at peak

The data for the contents of Si-H derived from the wagging mode are scattered, because it is difficult to separate the absorption for the Si-H wagging mode (630 1/cm) from the absorption for Si-N asymmetric (850 1/cm) and symmetric (450 1/cm) modes. The content of Si-H derived from the stretching mode increases with the ammonia gas fraction, while that derived from the wagging mode does not. This discrepancy is probably caused by a change in the oscillator strength of the Si-H stretching vibration.

It is useful to evaluate the absorption coefficient for Si-N vibration in order to obtain the information on the N content. Figure 3.3 shows the infrared optical absorption coefficient of Si-N, Si-H, and N-H vibrations as a function of the ammonia gas fraction x = $NH_3/(SiH_4 + NH_3)$. Figure 3.4 shows the infrared absorption coefficient spectra for undoped a-SiN:H. The parameter in the figure is the ammonia gas fraction x = $NH_3/(SiH_4 + NH_3)$. It is found that as the NH_3 gas fraction increases, the absorption coefficients of Si-N, Si-H and N-H modes increase. This implies that as the NH_3 gas fraction increases, a larger number of N atoms will be involved into the film. It should be noted that these films also contain hydrogen atoms of about 20 - 30 % at atomic number. The increase in the number of N atoms should effect in the enlarging of the optical energy gap of a-SiN:H [16].
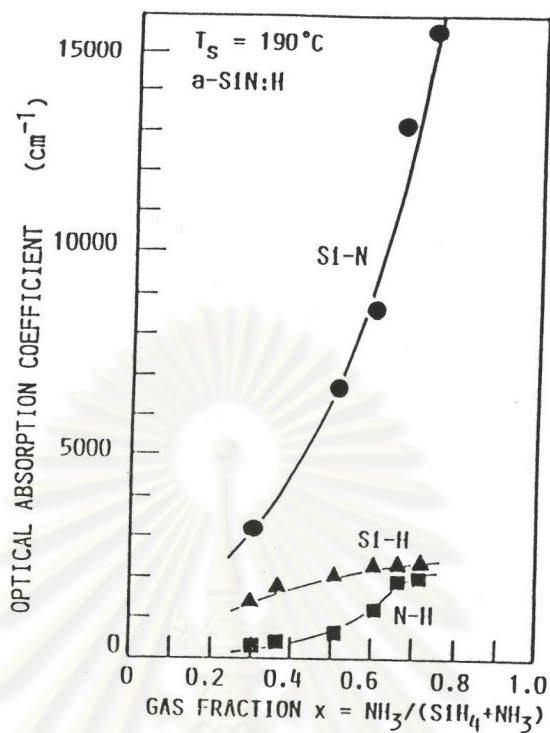
Figure 3.3   Infrared optical absorption coefficient of Si-N, Si-H, and N-H vibrations as a function of the ammonia gas fraction x = NH₃ / (SiH₄ + NH₃).
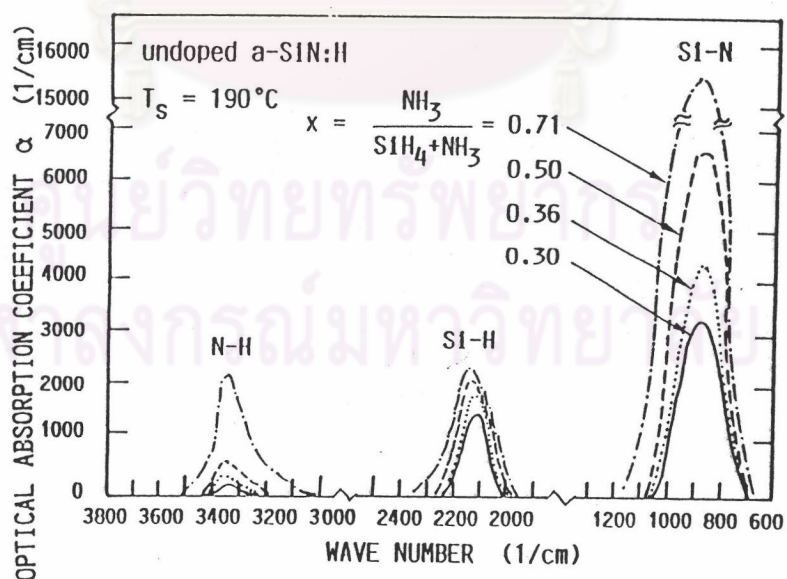

Figure 3.4   Infrared optical absorption coefficient spectra for undoped a-SiN:H.

3.2.2 Measurement of Dangling Bond Density in a-SiN:H Films by Electron Spin Resonance (ESR)

Electron spin resonance (ESR) is one of the few experiments which give structural information about defects. When a quantum state is occupied by a single electron, the two states of the Pauli pair are normally degenerated, but are split by a magnetic field. Paramagnetic and ESR are the result of the transitions between the split energy levels. The transition occurs at microwave frequencies for the usual magnetic fields. The strength of the microwave absorption gives the density of the paramagnetic electrons and the ESR spectrum gives information about the local bonding structure. The technique is sensitive, being able to detect about 10^{11} spins and well suited for the measurement of low defect densities.

A few of study have been done on undoped a-SiN:H [19]. The purpose of this study is to use ESR for studying the structural properties and the film quality of undoped a-SiN:H films.

In this work, several undoped a-SiN:H samples with different gas fractions were prepared. Figure 3.5 shows an example of the ESR spectrum for undoped a-SiN:H prepared at the gas fraction $x = NH_3/(SiH_4 + NH_3) = 0.5$. Figure 3.6 summarizes the ESR spin density as a function of the ammonia gas fraction (x). It is found that the spin density of a-SiN:H increases from 10^{16} $1/cm^3$ to 10^{18} $1/cm^3$, when the ammonia gas fraction x increases from 0 to 0.7.

Figure 3.7 shows the g-value of a-SiN:H as a function of the ammonia gas fraction (x). The g-value decreases from 2.0055 to 2.0035 with increasing the ammonia gas fraction from 0 to 0.7. This variation might be due to the interaction of Si with surrounding N atoms.

The change of the g-value of the ESR signal can be explained in terms of the following model [6]. For simplicity, as shown in Fig. 3.8, let us assume two typical types of dangling bonds with three nearest-neighbor Si atoms, giving g = 2.0055 typical values for a-Si:H (a). The other is a Si dangling bond with three nearest-neighbor N atoms, giving g = 2.0030 typical values for a-SiN:H (b). As shown in Fig. 3.6, the spin density of Si dangling bonds increases with an ammonia gas fraction,
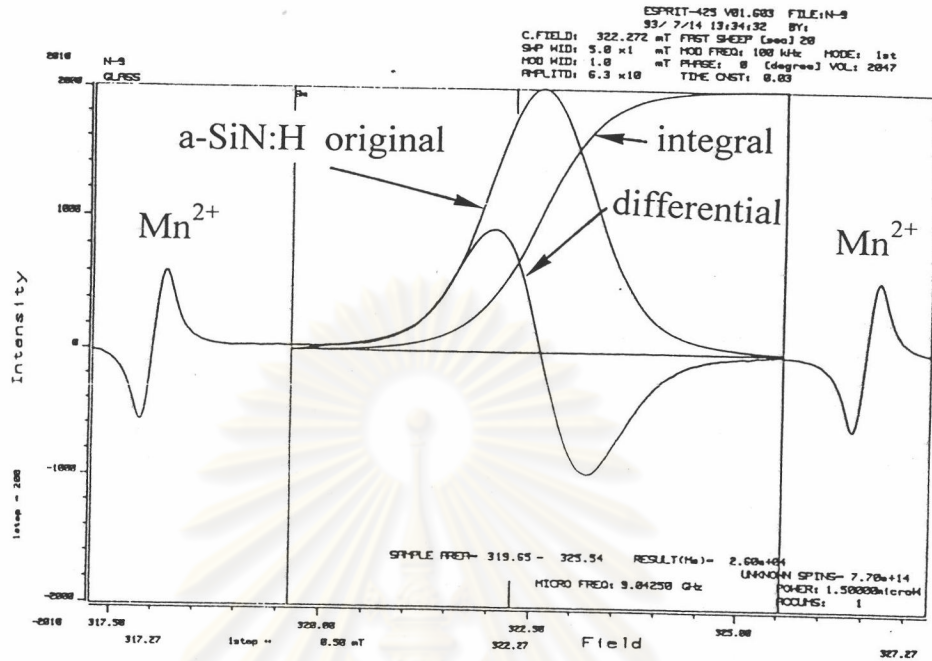
Figure 3.5   ESR spectrum for undoped a-SiN:H prepared at the ammonia gas fraction
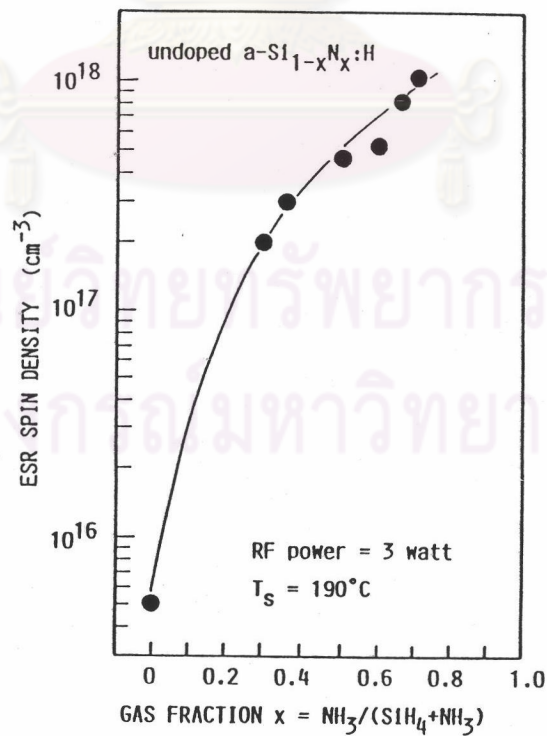$NH_3 / (SiH_4 + NH_3) = x = 0.5$

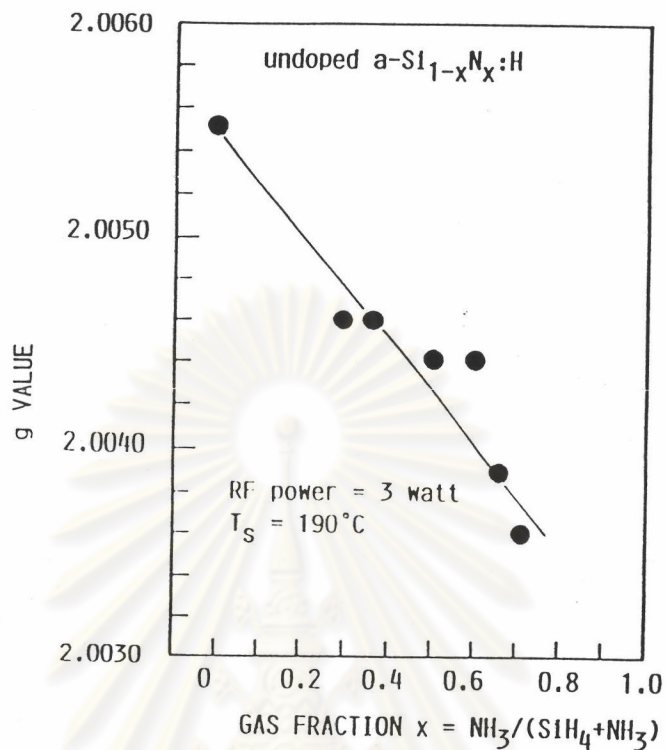Figure 3.6   ESR spin density as a function of the ammonia gas fraction (x).

Figure 3.7   G-value as a function of the ammonia gas fraction (x).
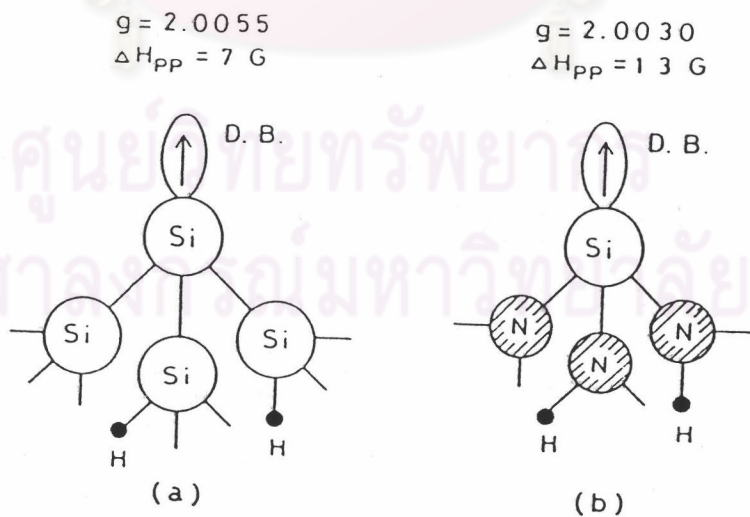

Figure 3.8   Two typical dangling bonds (D.B.) at different sites [6].

indicating that incorporation of N atoms with the covalent radius shorter than that for Si atoms induces stress in the amorphous network [20]. However, the bonding of H atoms to N atoms as shown in Fig. 3.8 (b) reduces the stress induced by N atoms, owing to the increase in the structural flexibility, resulting in a decrease in the density of Si dangling bonds with nearest-neighbor N atoms. Based on this model, the ratio of the density of dangling bonds of type (b) to that of Si dangling bonds of type (a) decreases with increasing N-H atom content, leading to the increase in the g-value.

Although the spin density of the undoped a-SiN:H is as high as 10^{17}-10^{18} 1/cm^3, the undoped a-SiN:H prepared in this work has good enough electronic quality to be used as the luminescent i-layer in the TFLED as will be shown in section 3.4-3.7.

3.3 Optical Properties of a-SiN:H Films
3.3.1 Optical Absorption Edge of a-SiN:H Films

In this work undoped a-SiN:H has been used as a luminescent active layer in the TFLED for the first time. One of the unique features of a-SiN:H is that the basic properties of the materials can be widely varied by controlling the film compositions. Therefore, it is possible to vary the optical energy gap of a-SiN:H in a wide range. This property matches very well with the requirement of the visible-light emitting device.

In this section, the results of the study on the optical absorption spectra near band edges for a-SiN:H having a wide range of nitrogen contents are presented and discussed.

Figure 3.9 shows the optical absorption coefficient spectra near the fundamental band edge for a-SiN:H. The parameter is the ammonia gas fraction x = $NH_3/(SiH_4+NH_3)$. It is found that as the ammonia gas fraction increases, not only the optical energy gap shifts to higher energy but also the magnitude of the absorption coefficient at the energy region below the exponential tail drastically increases. As will be shown in section 3.3.2, the luminescence in the a-SiN:H arises from the radiative recombination of carriers through the deep localized states below the
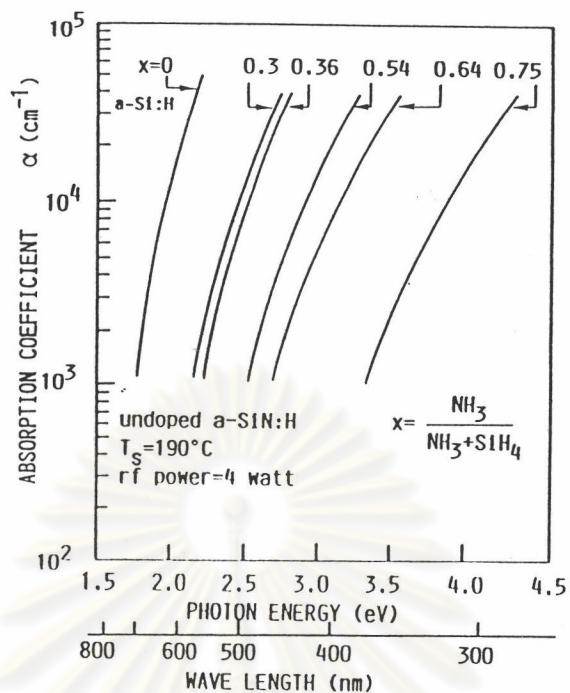
Figure 3.9 Optical absorption coefficient spectra near the fundamental band edge for a-SiN:H. The parameter is the ammonia gas fraction x = NH_3 / (SiH_4 + NH_3).
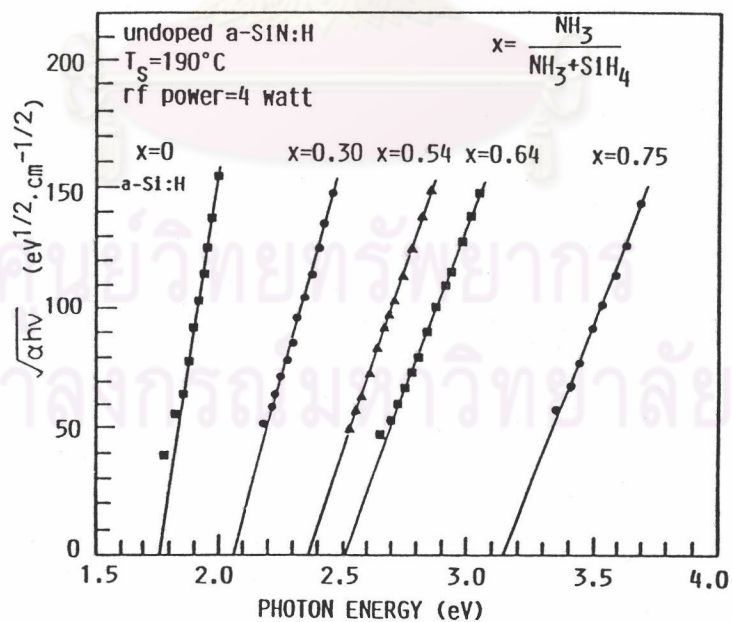

Figure 3.10 Tauc's plot for the determination of the optical energy gap of a-SiN:H.
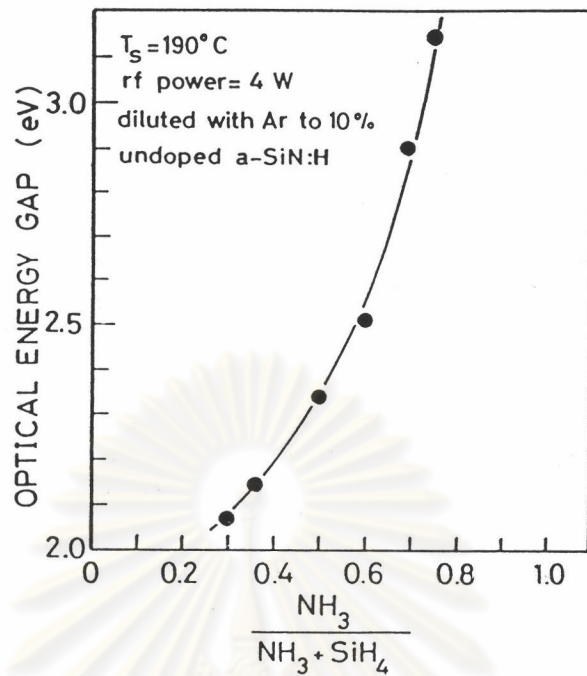
Figure 3.11 Relationship between the ammonia gas fraction and the optical energy gap of undoped a-SiN:H.
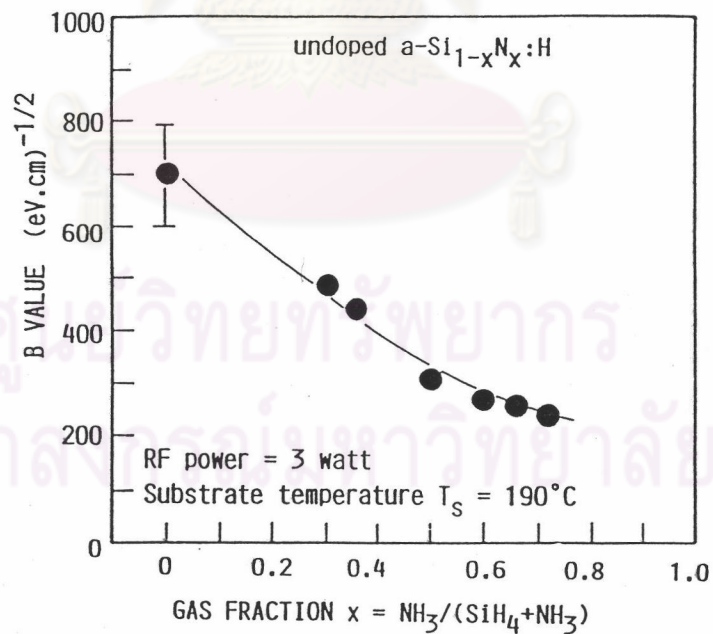

Figure 3.12 Relationship between B value and the ammonia gas fraction (x).

exponential tails. Therefore it is expected that the deep localized states will be useful to the luminescence.

Figure 3.10 shows Tauc plots for the determination of the optical energy gap of a-SiN:H. In the figure, the data are plotted in a straight line in an appropriate energy range. The extrapolation of the straight line to the energy axis gives the optical energy gap. It is found in Fig. 3.10 that as the ammonia gas fraction increases, the optical energy gap increases. The dependence of the optical energy gap on the ammonia gas fraction is summarized in Fig.3.11.

Figure 3.11 shows the relation between the ammonia gas fraction and the optical energy gap of undoped a-SiN:H. Here, the optical energy gap of undoped a-SiN:H was determined from the Tauc's plot of $(\alpha h\nu)^{1/2}$ vs $(h\nu)$. The optical energy gap of a-SiN:H increases monotonically from 2.07 eV to more than 3.09 eV with increasing the ammonia gas fraction x from 0.3 to 0.71. The data in Fig. 3.11 will be useful for the fabrication of the visible-light TFLED, since they give important conditions to obtain a-SiN:H with wide optical energy gap.

Figure 3.12 shows the relation between B-value and the fraction of ammonia gas (x). The B-value decreases as the fraction of ammonia gas x increases. This is due to a larger potential fluctuation caused by the incorporation of nitrogen atoms into the a-SiN:H network. It is generally considered that absorption coefficient spectra just around the energy gap reflect the distribution of tail states, especially in the valence band side.

3.3.2 Photoluminescence (PL) of a-SiN:H Films

Photoluminescence is a technique widely used in studying carrier recombination mechanisms and the localized states within the band gap of a semiconductor. It is particularly applicable to amorphous semiconductors with high densities of localized states [21-23]. It has been shown that there is an inverse correlation between luminescent intensity and electron spin resonance (ESR) spin density in a-Si:H [24-25]. In a luminescent process, electron-hole pairs are first excited, usually by externally injected photons (photoluminescence) or charge carriers

(electroluminescence). Electron-hole pairs then relax downward in energy (called thermalization) and eventually (in about 10^{-12} second) end up in band-edge localized states. Finally, they recombine either radiatively (luminescence) or nonradiatively (energy converted to heat). Dangling bonds and defects are predominant nonradiative recombination centers. By studying the relaxation process and intensity and spectral distributions of the radiated signal, one can obtain detailed information about nature of defects states [26].

Photoluminescent (PL) measurements of a-Si:H usually start at liquid helium temperature of about 4 K, the PL signal increases due to reductions in Auger recombinations of neighboring electron-hole pairs. The PL intensity reaches a peak at 50 to 100 K (depending on the sample) and decreases with temperature. There is no detectable PL signal in a-Si:H at room temperature because most of the photogenerated charge carriers recombine through the defects rather than from band tail to band tail. Usually there are two clearly observable PL peaks in a-Si:H a dominant peak near 1.4 eV and a smaller peak near 0.9 eV. The 1.4 eV peak is identified as a radiative tunneling transition between band-tail states. The 0.9 eV peak seems to originate from recombinations through defect states [22]. The interest in the photoluminescent properties of a-Si:H is mostly paid to the study of the nature of localized states, rather than to the exploration of a light emitting device, because the emission is almost in the infrared region.

Our interest in this work is to explore a visible light emitting diode, so we need a wider band gap material. One of the candidates as wide gap amorphous semiconductors is a-SiN:H, which was first prepared by Anderson and Spear [2] and H. Kurata et al. first reported that a-SiN:H shows visible photoluminescence [12]. In the design and fabrication of a visible-light thin film LED, it is important to know the basic properties of photoluminescence of wide gap a-SiN:H. The photoluminescence is also useful for the explanation of the electroluminesent characteristics of the amorphous TFLED.

In this section, the photoluminescent (PL) properties of undoped a-SiN:H having a wide range of optical energy gap from 2.07 eV to more than 3.09 eV are

presented. The results of the examinations of the dependence of PL on the excitation energy are also described and discussed.

3.3.2.1 Dependence of PL Spectra on Optical Energy Gap

Undoped a-SiN:H films were prepared by the RF glow discharge plasma CVD method from a mixture of silane and ammonia gases. The optical energy gap was varied from 2.07 eV to 3.09 eV by varying the ammonia gas fraction (NH_3/ (SiH_4+NH_3). Photoluminescent measurements were carried out at room temperature using a 3250 Å He-Cd laser as an excitation source.

Figure 3.13 shows photoluminescent spectra measured at room temperature of undoped a-SiN:H. The parameter is the optical energy gap of undoped a-SiN:H. The optical energy gap was changed by varying the ammonia gas fraction. The PL spectrum shows a single broad band. The emission color of the PL can be controlled from red to green by adjusting the optical energy gap from 2.07 eV to about 3.09 eV. The spectra shift toward higher photon energy with increasing the optical energy gap. At the same time the spectra tend to become broader, implying increased compositional fluctuations or an enhanced electron-phonon interaction.

Figure 3.14 summarizes the dependence of the peak energy of photoluminescent spectra on the optical energy gap for undoped a-SiN:H. It was observed that the PL peak energy (E_{PL}) has a good one-to-one correlation with the optical energy gap (E_{opt}). It should be noted that the PL peak energy usually shows a stoke shift lying at an energy lower than its corresponding optical energy gap. The stokes shift might be caused by the distortion of lattices in part and/or by the relaxation of carriers down into deep states before recombination take place.

The relationship between NH_3 gas fraction and optical energy gap and PL peak energy for a-SiN:H are summarized in Fig. 3.15. It is likely that as the optical gap increases; the value of E_{opt} - E_{PL} and the full width of PL spectrum become larger. This might imply that as the nitrogen content increases, the distribution of the radiative recombination centers becomes broader and deeper within the gap. The distribution of the radiative recombination centers in the gap can be further examined
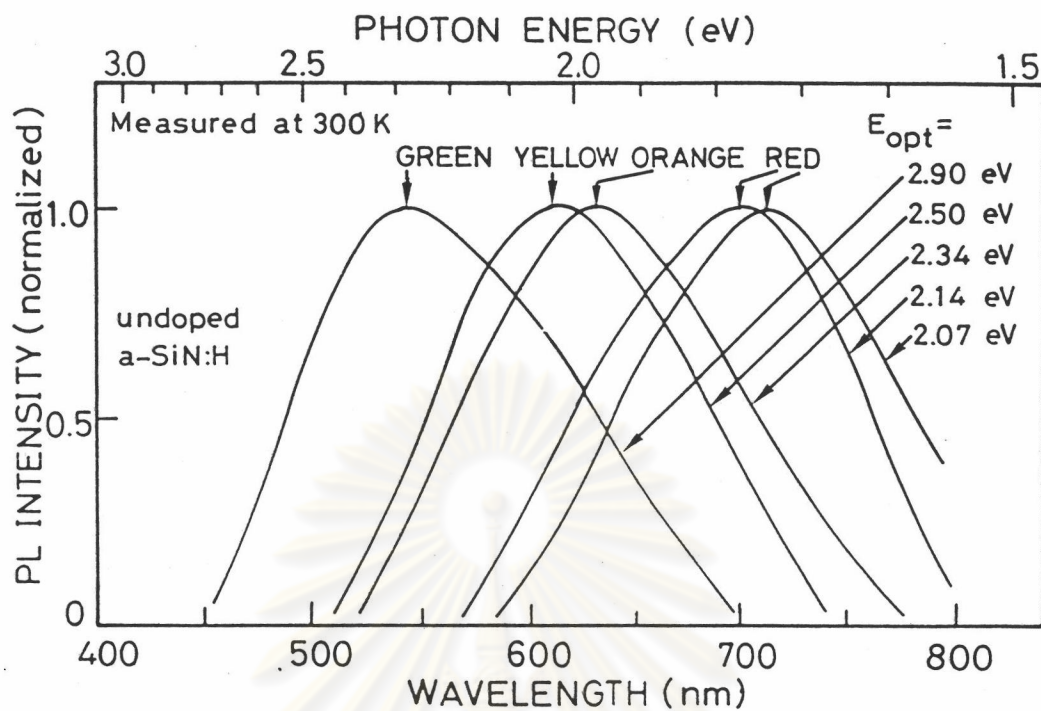
Figure 3.13 Photoluminescent spectra measured at room temperature of undoped a-SiN:H. The parameter is the optical energy gap of undoped a-SiN:H.
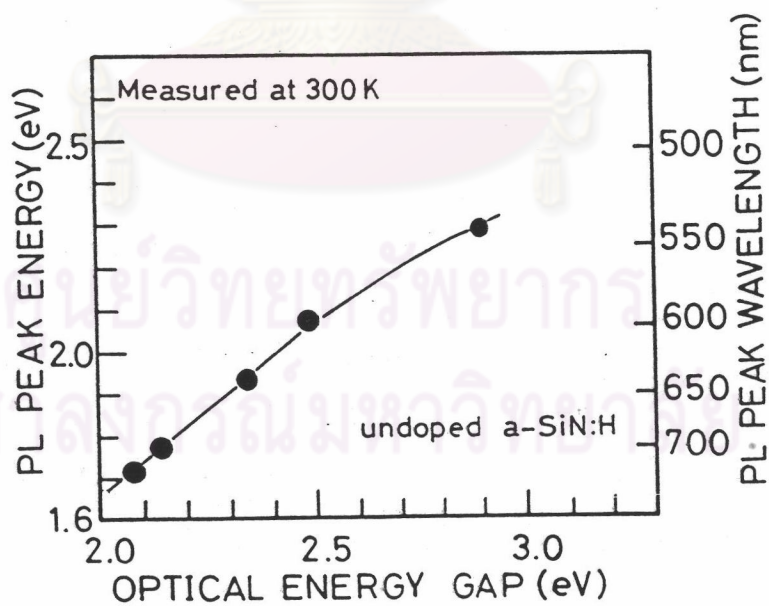

Figure 3.14 Dependence of the peak energy of photoluminescent spectra on the optical energy gap for undoped a-SiN:H.
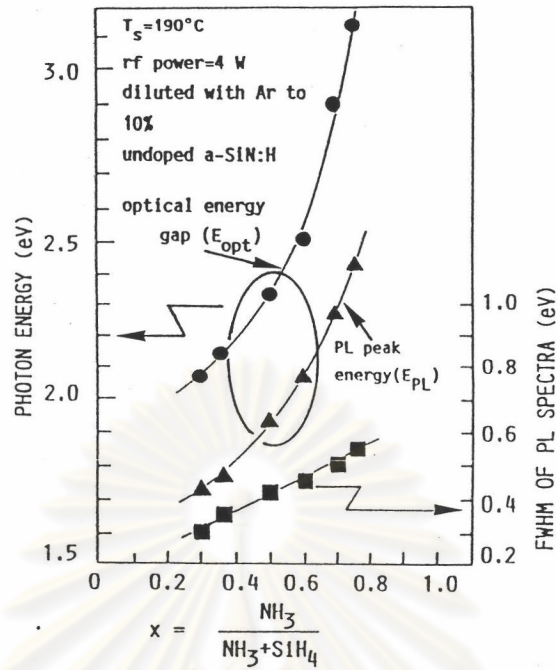
Figure 3.15 Relationship between NH_3 gas fraction and optical energy gap and PL peak energy for a-SiN:H.
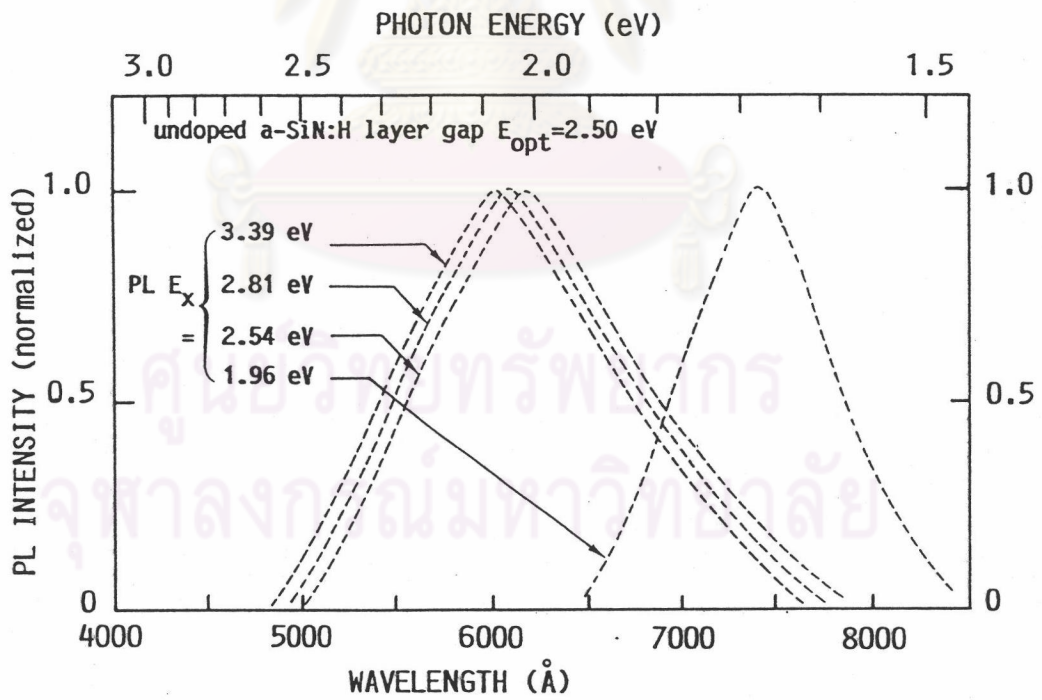

Figure 3.16 Room temperature dependence of the PL spectra on the excitation energy (E_X) for a-SiN:H having the optical energy gap of 2.50 eV.

by changing the excitation energy for PL measurement and this will be described in the next section.

3.3.2.2 Excitation Energy Dependence of PL Spectra

The photoluminescent process is generally considered as comprising three distinct events in sequences. First, an electron-hole pair is excited by the absorption of a photon. Second, the electron and hole relax down in energy by emitting a series of photon (thermalization), which usually ends up in band-edge localized states. Finally, there is recombination, either by radiative or by some nonradiative mechanisms.

The process of thermalization of carriers down the band tails is a characteristic feature of amorphous semiconductors. Therefore, the luminescent properties will depend in part on how fast the carriers move into the band tails. Several features of the luminescence exhibit the effect of the thermalization. It can be seen, for example, in the excitation energy dependence of PL spectra or time resolved spectra. The excitation energy dependence of PL for a-Si:H has been reported by a number of authors [27-29]. However, there has been no report on a-SiN:H, so far. In this section, a series of experimental investigations on the excitation dependence of PL spectra of a-SiN:H is presented.

The excitation lights used for investigating this dependence were the combination of cw 3250 Å, 4420 Å, He-Cd lasers, cw 4880 Å Ar laser, cw 6328 Å He-Ne laser and monochromated light from a Xe lamp. Figure 3.16 shows room temperature dependence of the PL spectra on the excitation energy (E_x) for a-SiN:H having the optical energy gap of 2.50 eV. All the spectra were measured at room temperature. As the excitation photon energy is decreased from 3.39 eV to 1.96 eV, the PL spectra shift to lower energy and the photoluminescent colors change from yellow to red.

Figure 3.17 summarizes the room temperature dependence of the PL peak energy on the excitation energy for various a-SiN:H. The optical energy gaps of a-SiN:H are 2.14 eV, 2.37 eV, 2.50 eV and 2.90 eV, respectively. As the excitation
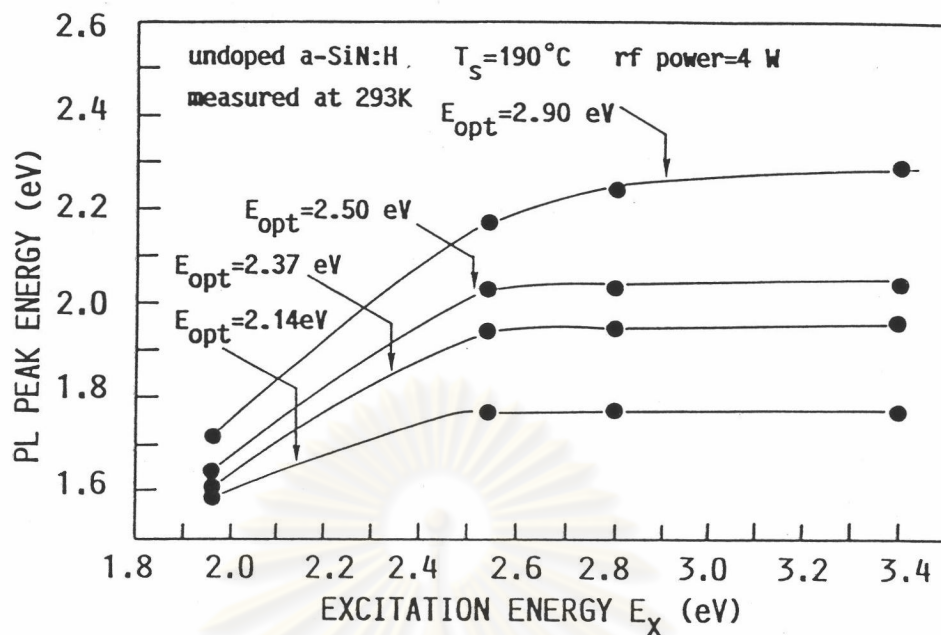
Figure 3.17 Room temperature dependence of the PL peak energy on the excitation energy for various a-SiN:H.
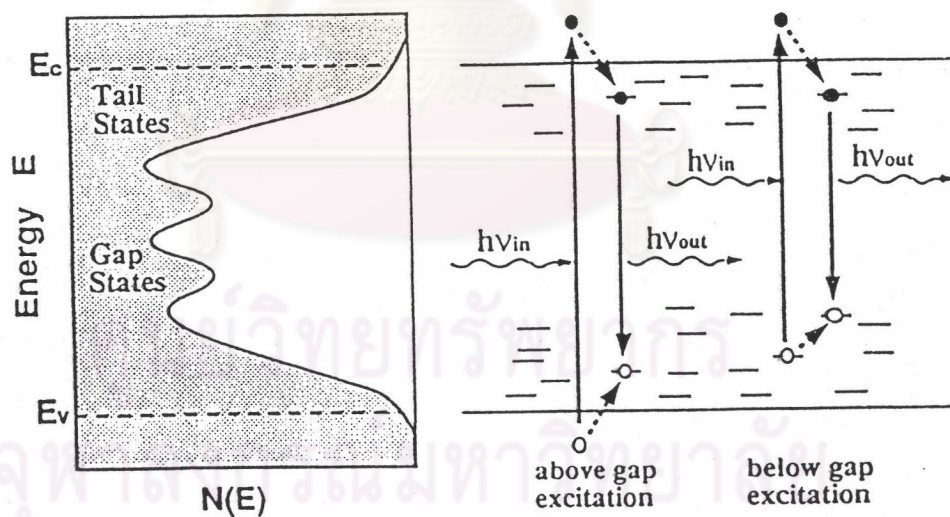

Figure 3.18 Schematic illustrations of (a) the density of states of a-SiN:H and (b) the excitation and recombination processes in a-SiN:H.

photon energy (E_x) is increased, the PL peak energy (E_{PL}) seems to saturate when the excitation photon energy exceeds the corresponding optical energy gap (E_{opt}).

The shift of the PL spectra observed in the case of the below-gap excitation might be understood in the same way as in a-Si:H [27-29], in term of a memory effect of the initial state of photo-excited carrier. Figure 3.18 show the schematic illustration of (a) the density of states of a-SiN:H and (b) the excitation and recombination processes in a-SiN:H. When the excitation photon energy is lower than the optical gap ($E_x < E_{opt}$), one or both carriers are excited into deep localized states in the gap. In this case, since thermalization of the photo-excited carrier up to conduction or valence band never occurs, the radiative transition retains a memory of the excited initial state and its energy.

When the excitation photon energy is higher than the optical gap ($E_x > E_{opt}$), the electrons and holes are excited sufficiently far into the bands that thermalization occurs, so that the luminescent peak shows no memory of the initial states. However, a detailed analysis of this process is complicated by the fact that the excitation involves the combined density of states of both band edges. Thermalization effects can also be seen in time-resolved luminescent spectra [30]. The luminescence shifts to low energy with increasing time delay, and this has been interpreted in terms of thermalization of carriers. The luminescence decay time for a-SiC:H has been found to be about 200 psec [30] much shorter than that of a-Si:H, which ranges from 1 microsec to 1 msec [31]. This observation is consistent with temperature-insensitive and efficient radiative transition in N-rich a-SiN:H in which excited electrons and holes are more tightly bound at the excited position and in deeper band-tail states than in a-Si:H. The fast decay time in a-SiN:H is attractive for achieving fast-response light emitting diodes.

The above observation on the excitation energy dependence of PL spectra provides important information for the discussion on the injection-electroluminescence properties of p-i-n junctions TFLED, as will be described in detail in section 3.6.

3.3.2.3 Effect of External Applied Electric Field on the PL Properties

The photoluminescent properties of amorphous semiconductors are influenced by external perturbation during the measurements, such as temperature, electric field, magnetic field, pressure, ect. The quenching of photoluminescent intensity by an applied electric field of 10^5 V/cm or greater has been reported by a number of authors [32-33]. The natural interpretation of the effect is the ionization of electron-hole pairs by the electric field and a good fit to a Poole-Frenkel expression is found [34].

The basic structure of the amorphous thin film LED (TFLED) employed in this work is the p-i-n junctions of amorphous silicon alloys. In this chapter a-SiN:H is used as the i-layer. The operation of the a-SiN:H TFLED is done by applying an electric field in the forward bias direction across the p-i-n layers. It will be pointed later in section 3.6 that most of the applied electric field will be dropped in the i-a-SiN:H layer. This electric field will degrade the luminescent efficiency, since the electric field will decrease the recombination probability of the electron-hole pairs. Therefore, it will be useful to study the basic properties of the effect of the electric field on the photoluminescence of a-SiN:H.

Figure 3.19 shows photoluminescence of a-SiN:H in case of (a) without biasing electric field and (b) with biasing electric field. As shown in Fig.3.19 (b) the electric field separates electrons and holes, so that the probability of the recombination of electrons and holes is decreased.

Figure 3.20 shows the dependence of photoluminescent efficiency on the electric field for a-SiN:H. The optical energy gaps of undoped a-SiN:H were 2.60 eV and 2.31 eV. The sample configuration used for the measurement was quartz substrate/ITO/a-SiN:H(3000 Å)/Al. It was confirmed that in the range of the electric field applied in the experiment, no current was injected into the a-SiN:H layer. The magnitude of PL intensity decreases down to about 50 % of the initial value as the electric field is higher than 1.5 x 10^6 V/cm. However, it is fortunate that the quenching of the PL of a-SiN:H seems to be less than that of a-Si:H . The small quenching of the PL seen in a-SiN:H is interpreted as a result of strong coulomb interaction of electron-hole pair due to the small dielectric constant of a-SiN:H. The
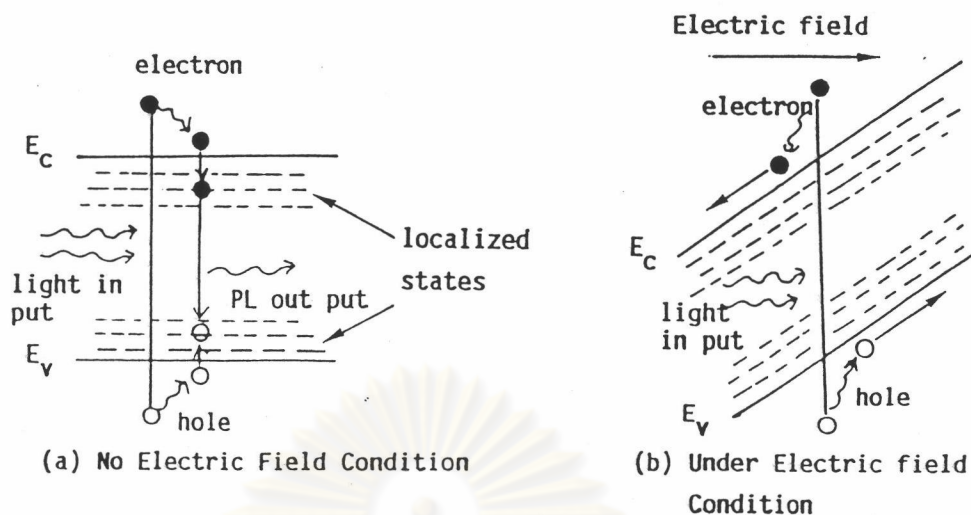
Figure 3.19 Photoluminescence of a-SiN:H in case of (a) without biasing electric field and (b) with biasing electric field.
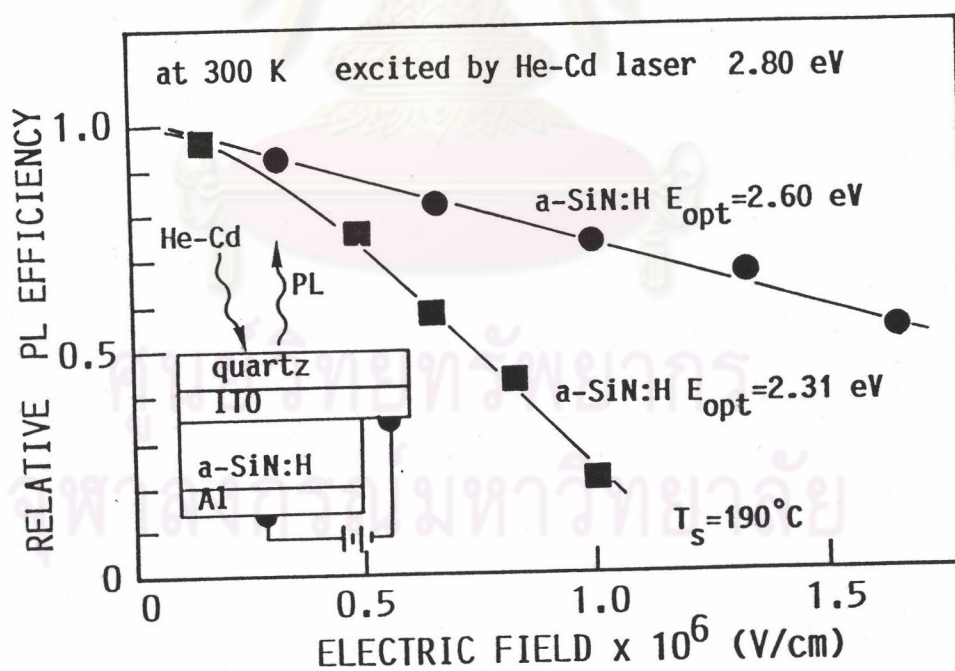

Figure 3.20 Dependence of photoluminescent efficiency on the electric field for a-SiN:H.

results of the experiment here suggest that in the viewpoint of the application of a-SiN:H to TFLEDs, it is of great importance to design and fabricate the devices in such a manner that the electric field in the i-layer should be as small as possible.

3.4   Structure and Fabrication of Thin Film Light Emitting Diode Having a-SiN:H as a Luminescent Layer

3.4.1 Basic Structure of a-SiN:H TFLED

The a-SiN:H thin film light emitting diode (TFLED) proposed in this work has a basic structure of glass/ITO/p-a-SiC:H/i-a-SiN:H/n-a-SiC:H/Al as illustrated in Fig. 3.21 where (a) is a cross section and (b) is a three dimensional view. A glass/ITO (Indium Tin Oxide) was used as a substrate. The thicknesses of the p-, i- and n-layers are 150 Å, 200 - 1000 Å and 500 Å, respectively. In the TFLED, the p- and n-a-SiC:H layers act as injectors of holes and electrons, respectively, into the a-SiN:H luminescent active i-layer.

The doping efficiency in a-SiN:H is much worse than in a-SiC:H. Therefore, in this work, p-a-SiC:H and n-a-SiC:H were used as the hole and electron injection layers. Under a forward bias condition, holes and electrons are injected from the p-a-SiC:H and n-a-SiC:H layers, respectively, into the i-a-SiN:H layer. The emission was observed through the glass substrate when the holes and electrons are radiatively recombined in the i-layer.

Figure 3.22   shows schematic band diagrams of p-a-SiC:H/i-a-SiN:H/ n-a-SiC:H heterojunction TFLED in (a) thermal equilibrium and (b) forward bias conditions. The injection electroluminescence was observed when the diode was positively biased. In order to obtain a visible luminescence, the optical energy gap of the i-layer has to be larger than 2.3 eV, as deduced from the results of the photoluminescent data in section 3.3.2. While the optical energy gaps of the p- and n-a-SiC:H layers should be chosen around 2.0 eV to ensure the effective valency controllability to p- or n-type.
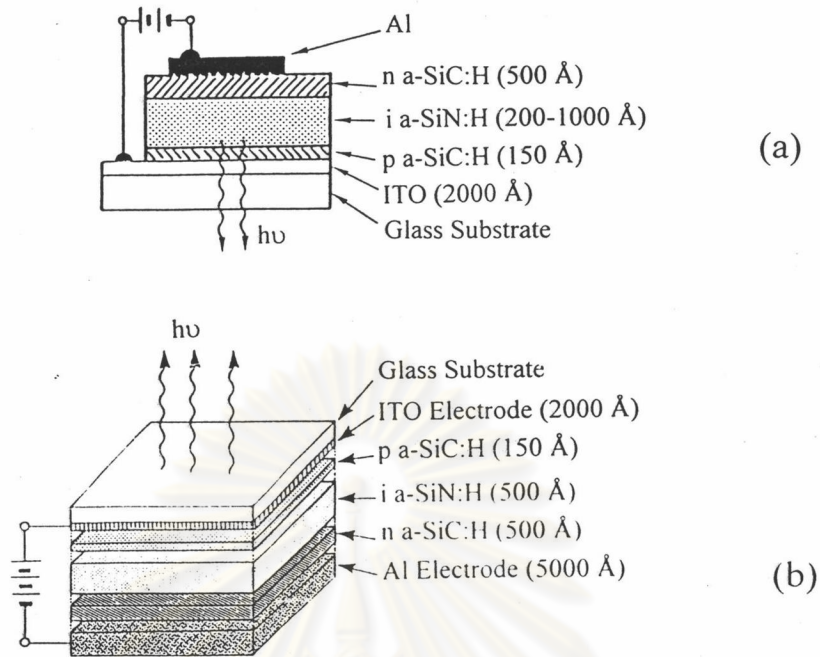
Al
n a-SiC:H (500 Å)
i a-SiN:H (200-1000 Å)
p a-SiC:H (150 Å)
ITO (2000 Å)
Glass Substrate
hυ

(a)

hυ

Glass Substrate
ITO Electrode (2000 Å)
p a-SiC:H (150 Å)
i a-SiN:H (500 Å)
n a-SiC:H (500 Å)
Al Electrode (5000 Å)

(b)

Figure 3.21 Basic structures of amorphous TFLED having a-SiN:H as a luminescent

layer illustrated in (a) cross section and (b) 3 dimensional view.

p a-SiC:H
(2.0 eV)

i a-SiN:H
(2.2-3.5 eV)

n a-SiC:H
(2.0 eV)

(a) Zero Bias

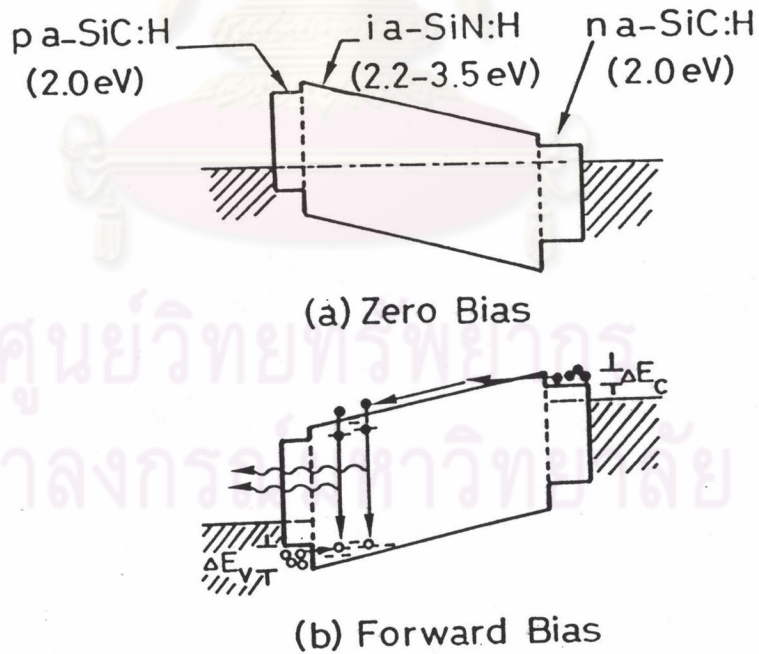ΔE_C

ΔE_V

(b) Forward Bias

Figure 3.22 Band diagrams of p-a-SiC:H/i-a-SiN:H/n-a-SiC:H heterojunction TFLED

in (a) thermal equilibrium and (b) forward bias conditions.

In section 3.4.2, some experimental data on the preparation and doping of p-a-SiC:H and n-a-SiC:H are described, and in section 3.4.3 fabrication process of the a-SiN:H TFLED will be presented.

3.4.2 Preparation and Characterizations of p- and n-a-SiC:H Films for Carrier Injection Layers

P- and n-type hydrogenated amorphous silicon carbide (a-SiC:H) were prepared by a conventional glow discharge plasma CVD system. SiH_4 and CH_4 diluted with H_2 to 10 % were used as gas sources. The substrate temperature (T_s) was 190 °C and the rf power was 3 - 4 watt. The total gas pressure during growing the film was 1 torr. The deposition rate of the p- and n-type a-SiC:H was about 0.20 to 0.40 Å/sec.

Figure 3.23 shows the relationship between the CH_4 gas fraction and the optical energy gap for undoped a-SiC:H. As the CH_4 gas fraction x increases from 0.2 to 0.8, the optical energy gap of undoped a-SiC:H increases monotonically from 1.95 eV to 3.50 eV. However, when the carbon content in a-SiC:H increases, the dangling bond density increases rapidly. The increase in the dangling bond density lead to the decrease in the doping efficiency as can understood in Fig. 3.24. Figure 3.24 shows the dependence of the dark conductivity on the optical energy gap for p-type a-SiC:H. The fermi level in the doped a-SiC:H can be evaluated by the activation energy of the ln σ_D vs 1/T plot as shown in Fig. 3.25. Figure 3.25 shows the dependence of the dark on the reciprocal temperature for p-type a-SiC:H. The fermi level of p-type a-SiC:H, having the optical energy gap around 2.0 to 2.10 eV, are approximately 0.3 - 0.4 eV. In this work, to ensure dark conductivity of the order of 10^{-8} (S/cm), p- and n-type a-SiC:H having the optical energy gaps constant at 2.0 eV were selected as the carrier injection layers in TFLEDs.

B_2H_6 and PH_3 (each diluted in H_2 , to 500 ppm) were used as dopant gas sources. During growing the film, boron was acceptor and phosphine was donor in the silicon alloy networks. The typical preparation conditions for p- and n- a-SiC:H layers are summarized in Table 3.2.
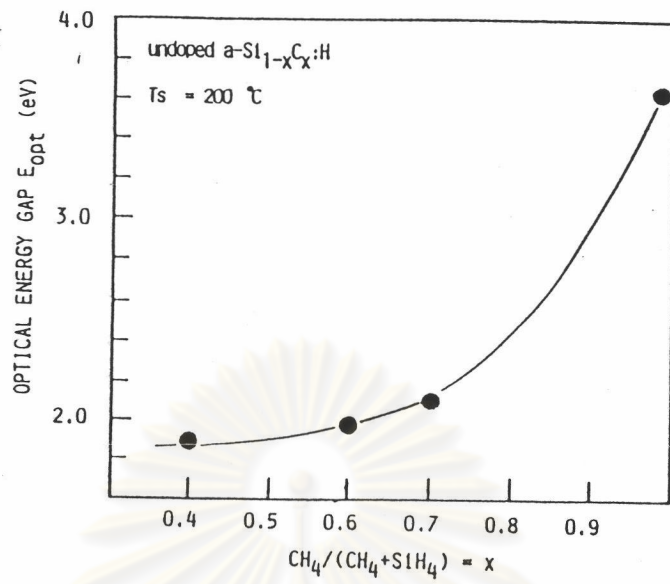
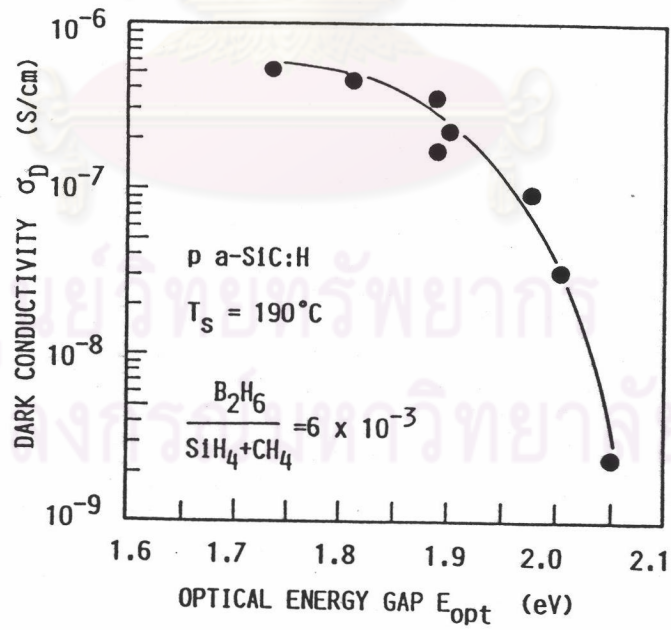Figure 3.23 Relationship between the CH$_4$ gas fraction and the optical energy gap of a-SiC:H.

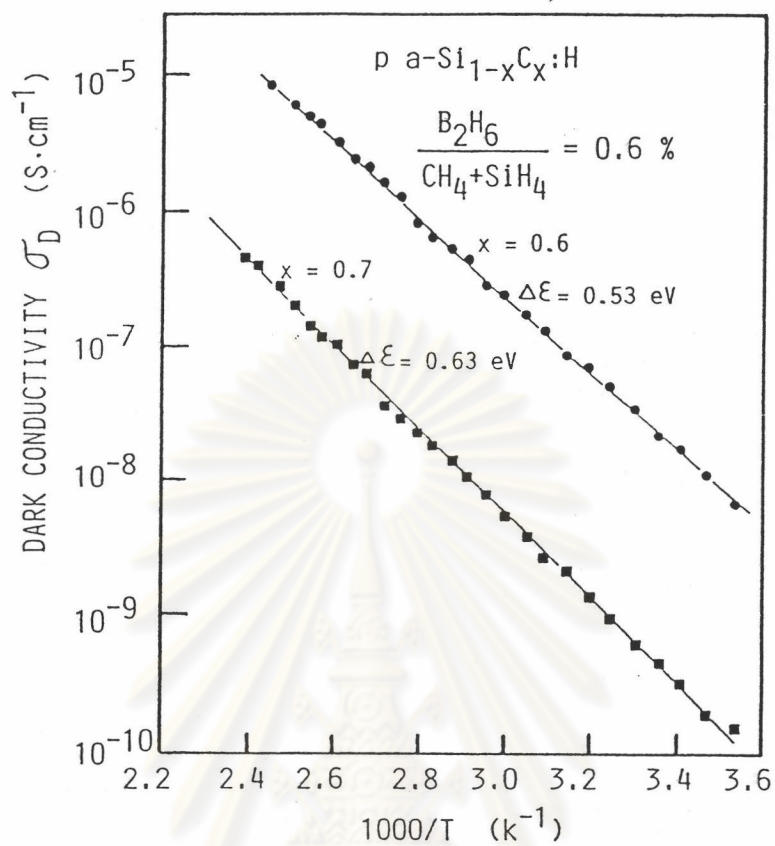Figure 3.24 Dependence of the dark conductivity on the optical energy gap for p-type a-SiC:H.

Figure 3.25 Dependence of the dark conductivity on the reciprocal temperature for p-type a-SiC:H.

Table 3.2 Typical preparation conditions of p- and n-type a-SiC:H.

RF Power	3-4 Watt, at 13.56 MHz
Substrate Temperature	190-200 °C
Total Gas Pressure	1 Torr
Gas for p a-SiC:H	$SiH_4 + CH_4 + B_2H_6$
Gas for n a-SiC:H	$SiH_4 + CH_4 + PH_3$
Gas Dilution	SiH_4 10 % + H_2 90 %
	CH_4 10 % + H_2 90 %
	B_2H_6 500 ppm in H_2
	PH_3 500 ppm in H_2
Doping Ratio	$B_2H_6/(SiH_4 + CH_4) = 6\times10^{-3}$
	$PH_3/(SiH_4 + CH_4) = 6\times10^{-3}$

3.4.3 Fabrication Process of a-SiN:H TFLED

The fabrication process of the a-SiN:H TFLED is shown in Fig. 3.26.

The transparent ITO electrode was evaporated by electron beam method. After cleaning the glass/ITO substrate, the substrate was put into the glow discharge plasma CVD system for the growth of the p-a-SiC:H, i-a-SiN:H and n-a-SiC:H layers, respectively. The back Al electrode was evaporated by a conventional heat resistive vacuum evaporator.
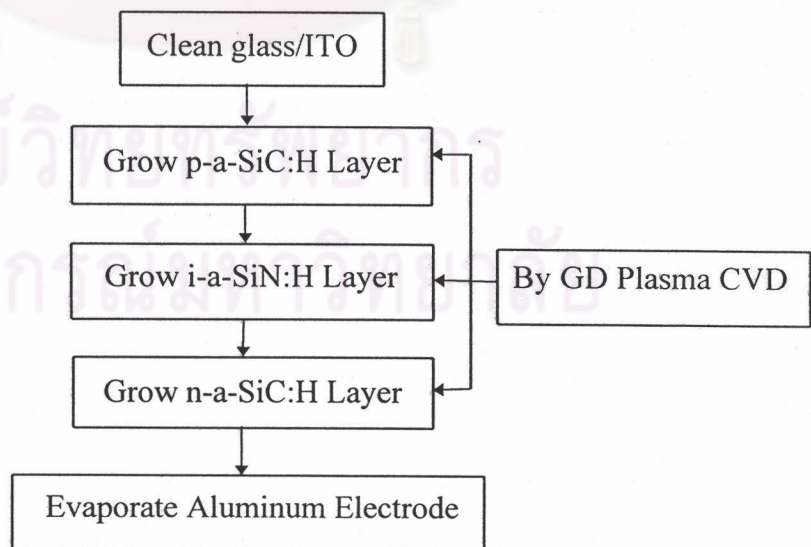

Figure 3.26 Fabrication processes of the a-SiN:H TFLED.

The typical preparation conditions of TFLED are summarized in Table 3.3.

Table 3.3 Typical preparation conditions of a-SiN:H TFLED

Power Source	C-Coupling, 13.56 MHz
RF Power	4 Watt
Substrate Temperature	190 ℃
Total Gas Pressure	1.0 Torr.
p-type a-SiC:H	$SiH_4/CH_4/B_2H_6$ = 1.5/3.5/0.03
i-type a-SiN:H	SiH_4/NH_3 = 6 ~ 10/3 ~ 4
n-type a-SiC:H	$SiH_4/CH_4/PH_3$ = 1.5/3.5/0.03
Cell Area	0.033 - 5 cm^2

3.5 Basic Characteristics of a-SiN:H TFLED

The a-SiN:H TFLED in this work has a structure glass/ITO/p-a-SiC:H/ i-a-SiN:H/n-a-SiC:H/Al. In the p-i-n junctions, p- and n-layers act as holes and electrons injection layers, respectively, and the i-layer acts as a luminescent active layer. The TFLED will emit light when it is forwardly biased. In order to obtain a visible luminescence, the optical energy gap of the emitting layer should be larger than 2.2 eV.

In section 3.5, basic characteristics of a-SiN:H TFLEDs, e.g., carrier injection mechanism, electroluminescent spectra, and the results of the optimization of the thickness of the i-a-SiN:H layer are reported. The dependence of the emission on the frequency of the pulse-mode operation (pulse modulation) was also investigated and discussed.

3.5.1 Carrier Injection Mechanism in a-SiN:H TFLED

a-SiN:H TFLED developed in this work has a structure of glass/ITO/ p-a-SiC:H/i-a-SiN:H/n-a-SiC:H/Al. In order to show that the device exhibits a diode characteristic, the relation between the current and the voltage was examined. The semilogarithmic curves of current density (J) versus applied voltage (V) measured at room temperature for the red and orange TFLEDs are shown in Fig. 3.27.

Figure 3.27 shows room temperature J-V curves for two a-SiN:H TFLEDs. The optical energy gaps of the i-a-SiN:H layer in the upper (red emission) and lower (yellow) TFLEDs are 2.50 eV and 2.90 eV, respectively. A rectification ratio of more than 10^2 is obtained at 8 V for the TFLED of which the optical energy gap of the i-a-SiN:H layer is 2.50 eV. It is noted that when the optical energy gap of the i-layer increases, the threshold voltage tends to increase. This might be partly due to the increase of series resistance in the i-a-SiN:H layer itself and to the increase of the notch barrier heights at both p/i and i/n interfaces.

The emission from the red TFLED can be observed when the current density is higher than 10^{-2} A/cm^2. The high forward current density above 10^{-2} A/cm^2 is thought to be due to the field-tunneling emission processes of holes and electrons through the notch barriers at p/i and i/n interfaces, respectively.

Next, a brief discussion on the carrier injection and transport mechanisms in the a-SiN:H/a-SiC:H p-i-n junctions is made.

Due to the difference in the optical energy gaps of the p-, i- and n-layers, there exist notch barriers at the p/i and i/n interfaces. In this kind of band structures, there are two possible processes of carrier injections into the i-layer.

1) If carriers have higher thermal energy than the barrier height, they can cross the barriers. This process is called as a "thermionic emission". In the developed TFLED, this process would play only a minor role since the barrier heights at the p/i and i/n interfaces are much larger than the thermal energy of carriers at room temperature.

2) Another process considered here is a field-tunneling through the barriers under a high electric field. It is strongly considered that this is the main process for the carriers to be injected into the i-layer.

Now, we will discuss on the field-tunneling process and show that the field-tunneling injection dominates the current flow in the TFLEDs.

If a tunneling injection dominates the current flow, the junction current J is expected to follow the expression of Flower-Nordheim ;
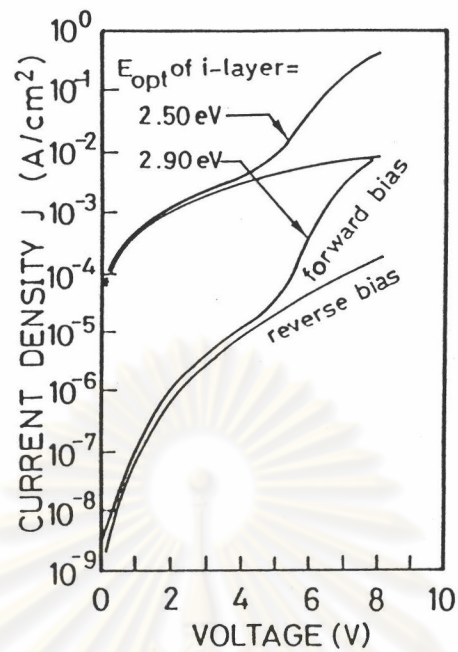
Figure 3.27 Room temperature J-V curves for two a-SiN:H TFLEDs.

The optical energy gaps of the i-a-SiN:H layer in the upper (red emission)

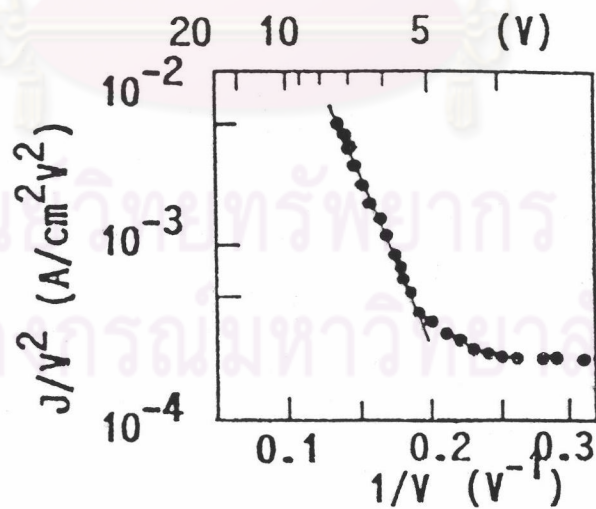and lower (yellow) TFLEDs are 2.50 eV and 2.90 eV, respectively.

Figure 3.28 Room temperature plot of log (J/V^2) vs 1/V for a red a-SiN:H TFLED.

$$J \quad \propto \quad E^2 \exp\left[\frac{-4\sqrt{2m^*}(\phi_B)^{3/2}}{3q\hbar E}\right] \qquad (3.2)$$

where E : the applied electric field across the i-layer in forward direction,

m^* : the effective mass of carrier,

q : the electron charge,

$\hbar$: $h/2\pi$,

ϕ_B : the barrier height for the tunneling, where in the a-SiN:H p-i-n junction corresponds to the conduction band discontinuity (ΔE_c) at the i/n (for electrons) or the valence band discontinuity (ΔE_v) at the p/i (for holes).

With an assumption that the applied electric field is uniformly distributed through the i-layer of the thickness d, equation (3.2) indicates that log (J/V^2) should have a linear dependence on 1/V. Figure 3.28 shows a plot of log (J/V^2) vs 1/V for the red a-SiN:H TFLED. The thickness of the i-layer is 500 Å. The electroluminescence (EL) is observed at the forward voltage higher than about 5 V. In this region, the plot of log (J/V^2) linearly depends on 1/V, showing an evidence of the tunneling injection process in the TFLED.

The barrier height for tunneling can be evaluated from the slope of the linear plot according to equation (3.2). Assuming that the carrier effective mass is equal to the free electron mass, the barrier height of the TFLED (red) in Fig. 3.28 is estimated to be about 0.26 eV. It is worth to say here that this value is close to the conduction band discontinuity at the i/n interface (ΔE_c) evaluated by the internal-photoemission measurement.

What we learn from these results is that the dominant current across the junctions arises from the injected electrons rather than holes. Hole current is considered to be only a minor component because the barrier height for holes to tunnel (ΔE_v) is larger than that for electrons by a factor of 2-3. However, since luminescence is based on radiative recombination of both electrons and holes injected

into the i-layer, the hole injection process will play a central role in determining the EL properties, as will be discussed in the following section.

3.5.2 Electroluminescent (EL) Spectra

A series of a-SiN:H TFLEDs consisting of the i-layers with different optical energy gaps has been fabricated. By changing the optical energy gap of the luminescent active i-layer from 2.50 eV to 2.90 eV, we have succeeded in the fabrication of red and yellow color emitting TFLEDs.

Figure 3.29 shows the EL spectra for two a-SiN:H TFLEDs measured at room temperature. The optical energy gaps of the i-a-SiN:H layers are 2.50 eV (red emission) and 2.90 eV (yellow emission). NH_3 was used as the nitrogen source gas in the i-layer. The forward injection current for the measurement is 800 mA/cm^2. For the TFLED of which the optical energy gap of i-layer is 2.50 eV, the EL spectrum peaks at 1.80 eV (red emission), with full width at half maximum (FWHM) = 0.26 eV. The TFLED of which the optical energy gap of the i-layer is 2.90 eV exhibits a broad band peaking around 2.20 eV (yellow emission) with FWHM = 0.58 eV. The electroluminescence from these samples are bright enough to be observed in a dim room.

Figure 3.30 summarizes the dependence of the peak energy of EL spectra (E_{EL}) on the NH_3 gas fraction during the preparation of the i-layer. The corresponding optical energy gap (E_{opt}) and the peak energy of the PL spectrum (E_{PL}) of a-SiN:H identical to the one used in the p-i-n TFLED are also shown for comparison. It is seen in Fig. 3.30 that the peak energies of EL spectra are, somewhat, lower than those of the PL spectra, and they seem to saturate at around 1.80 eV as the optical energy gap is wider than 2.90 eV.

In order to interpret why the peak energies of EL spectra are lower than those of PL spectra, the excitation photon energy (E_x) dependences of photoluminescence spectra of undoped a-SiN:H film has been investigated. Figure 3.31 shows the PL spectra excited by various excitation photon energies for undoped a-SiN:H film with the optical energy gap E_{opt} = 2.50 eV. For comparison, the EL spectrum (solid line)
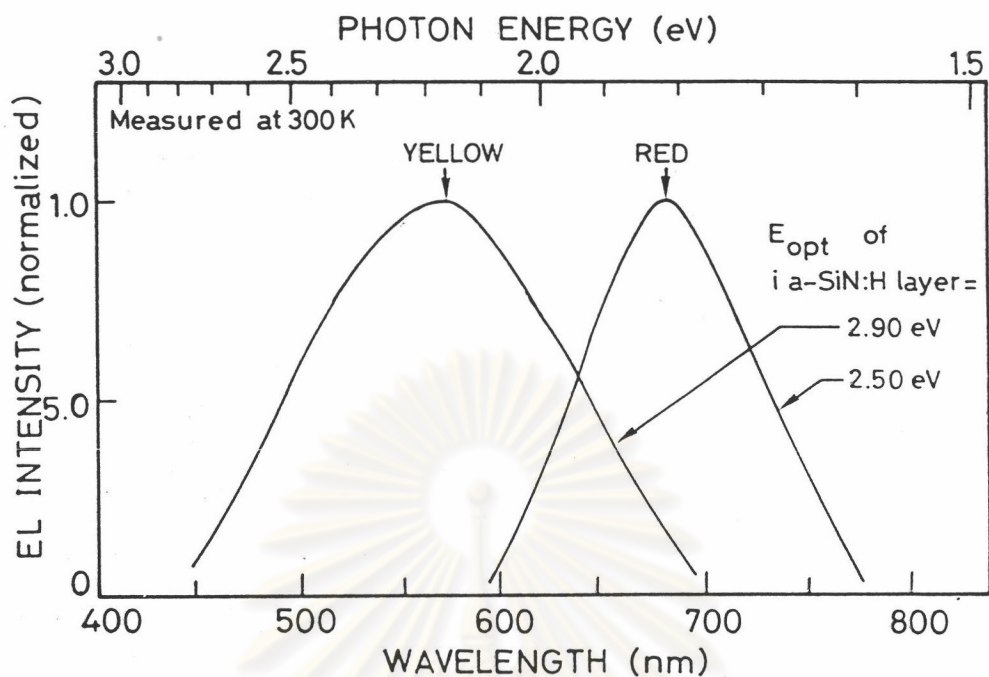
Figure 3.29 Room temperature EL spectra for two a-SiN:H TFLEDs. The optical energy gaps of the i-a-SiN:H layers are 2.50 eV (red emission) and 2.90 eV (yellow emission).
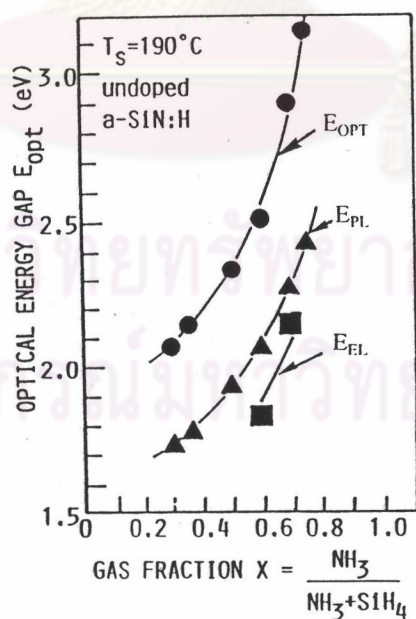

Figure 3.30 Dependence of the peak energy of EL spectra (E_{EL}) on the NH_3 gas fraction during the preparation of the i-layer.
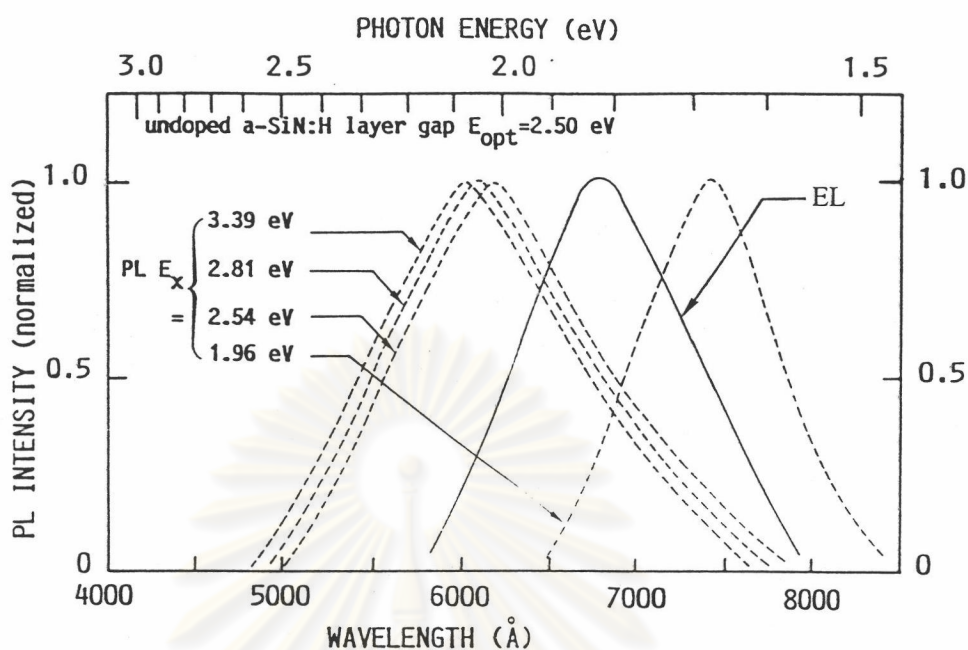
Figure 3.31 PL spectra excited by various excitation photon energies for undoped a-SiN:H film with the optical energy gap $E_{opt} = 2.50$ eV.
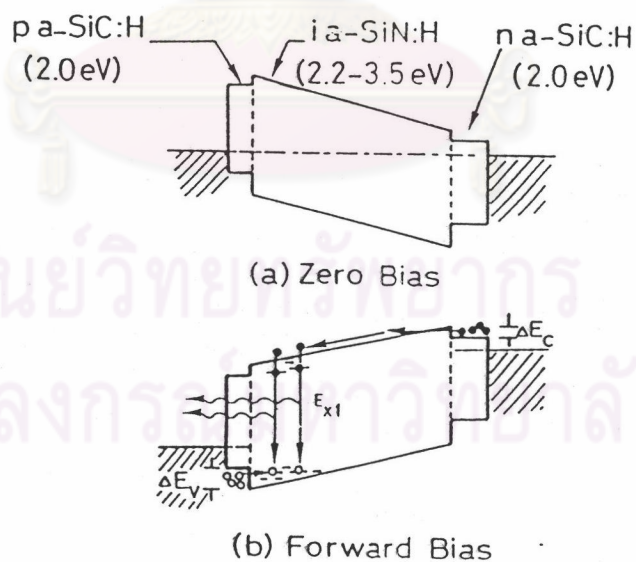

Figure 3.32 Schematic illustration of excitation energy E_x of electron-hole pairs in a-SiN:H.

of a TFLED of which the optical energy gap of i-layer = 2.50 eV is also shown in the figure. When E_x is decreased, the PL spectra shifts towards the lower photon energy region, and when E_x = 2.20 eV, the PL spectrum almost exhibits the same line shape as the EL spectrum. The shift of the PL spectra observed in the region at the below-gap excitation might be understood in the same way as in a-Si:H [28] in terms of a memory effect of the initial state of the photo-excited carriers as has been discussed in details in section 3.3.

The results obtained in the Fig. 3.30 and Fig. 3.31 imply that the EL peak photon energy would be limited not only by the optical energy gap of the i-layer but also by the excitation energy of the electron-hole pairs, that is the injection energy level of electrons and holes from the n- and p-layers. It has been shown that the tunneling injection process dominates the current flow in the TFLEDs, and electrons are injected through the notch barrier into the conduction band in the i-layer. In contrast, holes are likely to be mostly injected into the deep tail-states of the valence band edge of the i-layer and recombine with free electrons via the tail-states before they are thermalized into the valence band.

For example, with the optical energy gaps of the p- and i-layers = 2.0 eV and 2.50 eV, the barrier height for holes to tunnel is about 0.30 eV. Then the excitation energy E_x of electron-hole pairs as shown in Fig. 3.32 will be E_x = 2.50 - 0.30 = 2.20 eV. With the excitation photon energy E_x of 2.20 eV, the PL peak (E_{PL}) lies around 1.80 eV, being consistent with the peak energy of the EL spectrum, as shown in Fig. 3.31.

The results in this section suggest that if we can improve the injection energy level of holes, we might be able to shift the EL spectra to higher energy and also to improve the EL intensity.

3.5.3 Relationship Between Brightness and Current Injection Density of a-SiN:H TFLED

Figure 3.33 shows relationship between the brightness (B) and the injection current density (J) for the red and yellow a-SiN:H TFLEDs. The maximum
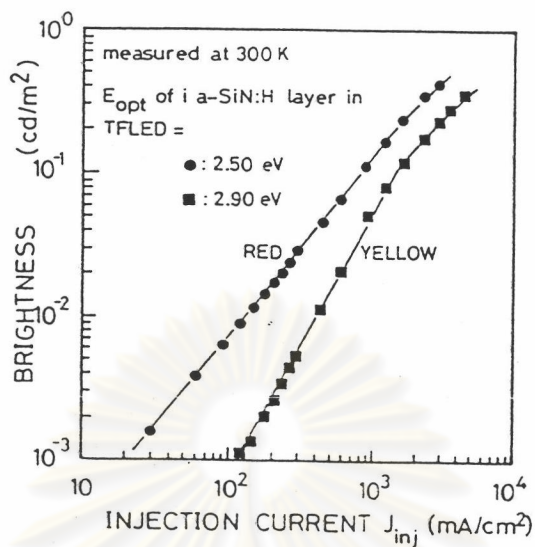
Figure 3.33 Relationship between the brightness (B) and the injection current density
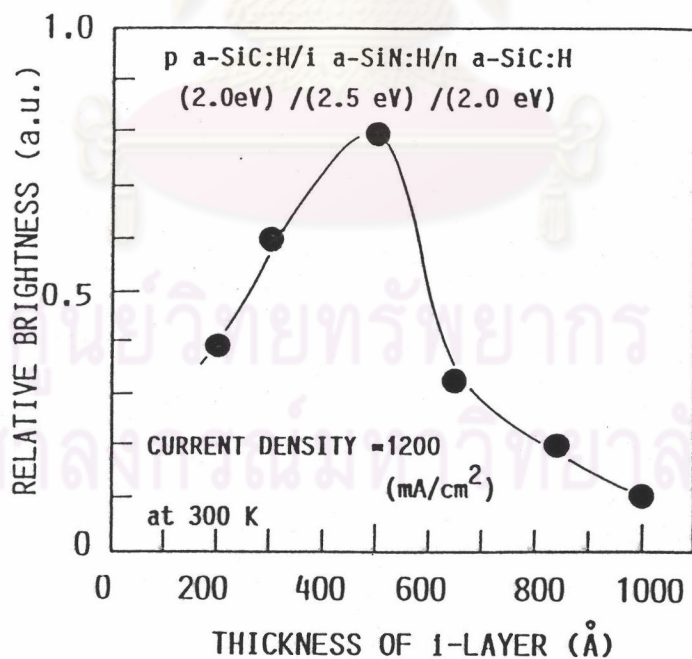(J) for the red and yellow a-SiN:H TFLEDs.

Figure 3.34 Dependence of the EL intensity on the thickness of the i-a-SiN:H layer for
the red TFLEDs.

brightness obtained was about 0.7-0.8 cd/m^2 at the current injection density of 2000-3000 mA/cm^2. The brightness (B) varies with the injection current density as $B \propto J^n$, where the exponent n is close to unity. It was pointed out for the case of a-SiC:H TFLED [35] that the exponent n was also unity and it was interpreted that the electroluminescent mechanism in the a-SiC:H TFLED was a classical monomolecular recombination or tail-to-tail states recombination process. Since the band diagram of a-SiN:H TFLED employed in this work is similar to that of a-SiC:H TFLED , it may be plausible that the EL mechanism in a-SiN:H TFLED should also be either a classical monomolecular recombination or tail-to-tail states recombination process.

Another interesting result observed in a-SiN:H TFLEDs in Fig. 3.33 is that the brightness of the TFLED with narrow optical energy gap i-layer is higher than the TFLED with wide optical energy gap i-layer. The experimental result for the a-SiN:H TFLED in this work obtained in the opposite direction of the case of the a-SiC:H TFLED as discussed in the literature [35]. In the case of the a-SiN:H TFLED, it is shown in section 3.2 that as the optical energy gap (N content) of a-SiN:H increases, the spin density increases. Therefore, the decrease in the brightness of the a-SiN:H should be due to the increase in the spin density of the i-layer. Another reason might be due to the increase in the notch barrier heights at the p/i and i/n interfaces. This is because as the notch barrier heights increases, the necessary electric field for the carrier to tunnel has to be increased, therefore, the high electric field will decrease the probability of the recombination of the injected carriers.

3.5.4 Optimization of the Thickness of i-Layer

In general, to obtain a high EL intensity (brightness), a thicker i-layer (that is a larger volume of radiative recombination centers) is required. Since the dominant current across the a-SiN:H TFLED (p-a-SiC:H/i-a-SiN:H/n-a-SiC:H junctions) is a tunneling current, a thick i-layer should generally limit the probability of tunneling due to a lowering of the electric field for tunneling. The trade-off between these two factors, then determines the thickness dependence of the EL intensity. In this section,
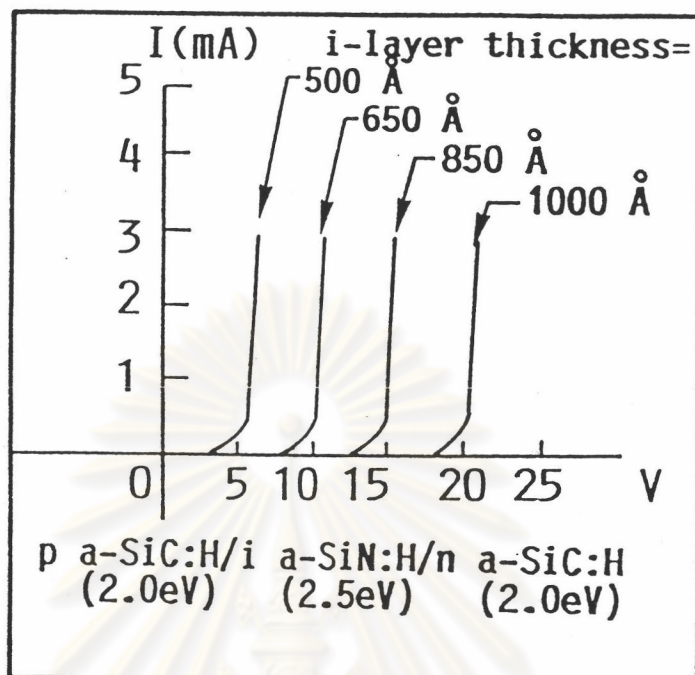
Figure 3.35 I-V curves of a-SiN:H TFLEDs with different thicknesses of the i-layers.

ศูนย์วิทยทรัพยากร
จุฬาลงกรณ์มหาวิทยาลัย

a series of experimental data on the dependence of EL intensity on the thickness of i-layer as well as a simple theoretical analysis are described [17].

Figure 3.34 shows the dependence of the EL intensity on the thickness of i-a-SiN:H layer for the red TFLEDs. The optical energy gap of the i-a-SiN:H layer here is 2.50 eV. The thickness of the i-layer was changed from 200 Å to 1000 Å. The current density for the measurement of the EL intensity was kept constant at 1200 mA/cm^2. It is found that the EL intensity becomes maximum at the thickness of about 500-600 Å. Details of the calculation of the optimization of thickness of the i-layer are described in appendix B.

Figure 3.35 shows the I-V curves of a-SiN:H TFLEDs with different thicknesses of the i-layers. The thickness of the i-layer was changed from 500 Å to 1000 Å. It is found that the threshold voltage increases as the thickness of the i-layer increases. And what is more interesting is that as the thickness increases twice from 500Å to 1000Å, the threshold voltage increases by a factor of 4 from 5 V to 20 V. If the current transport in the TFLED is simply dominated by the series resistance of the i-layer, the threshold voltage should be expected to increase by a factor of 2. Therefore, the result in Fig. 3.35 should imply that the tunneling process have to be taken into account. And another interesting discussion is that the high electric field will quench the EL intensity. Therefore, the EL intensity of the TFLED with the thickness of the i-layer of 1000 Å is smaller than that with the thickness of the i-layer of 500Å.

3.5.5 Dependence of EL Intensity on the Frequency-Modulation

For the application of a-SiN:H TFLED in optical communication and practical displays, the frequency response is one of the important characteristics. The frequency response is basically determined by the diffusion capacitance, carrier lifetime, the depletion layer's capacitance and differential resistance [36].

In this work, an investigation has been done on the dependence of the EL intensity of the a-SiN:H TFLED on the frequency modulation.

Figure 3.36 shows the typical light output waveform response to an input square-wave current pulse for the p-a-SiC:H/i-a-SiN:H/n-a-SiC:H junction yellow TFLED. In the measurement, the duty cycle of the current pulse was 50 % and the modulation current amplitude was kept constant. (The rms value of current was set at 666 mA/cm^2 for the area = 0.033 cm^2). It is found that the rise time and fall time of the light output signal are of the order of several microsecond.

Figure 3.37 shows the dependence of the EL intensity on the modulation frequency in the of 100 Hz to 1 MHz. The results show that the EL intensity is almost constant even though the frequency is as high as 1 MHz.

If it is generally defined in LEDs that a cut-off frequency f_c is the frequency that the EL intensity drops to half of its low frequency value [36], that is:

$$P^2(f_c) = \frac{1}{2} P^2(f = 0) \tag{3.3}$$

$$P(f_c) = 0.7 P(f = 0) \tag{3.4}$$

Then we get:

$$f_c = 1 / (2\pi\tau) \tag{3.5}$$

Here τ: Radiative recombination life time of carriers

If we assume that the cut-off frequency f_c of the a-SiN:H TFLED is in the range of 5 MHz to 100 MHz, then the radiative recombination lifetime of the injected carriers appears to be the order of 10^{-8} - 10^{-9} sec. This value is smaller than the carrier transit time across the i-layer.

The fact that the intensity of the light output does not decrease even at the frequency of 1 MHz indicates that the a-SiN:H TFLED can be operated and scanned up to such a high frequency. In general displays, the frequency of scanning signal is the order of kHz. Therefore, it is confirmed in this section that the a-SiN:H TFLED satisfies this requirement [17].
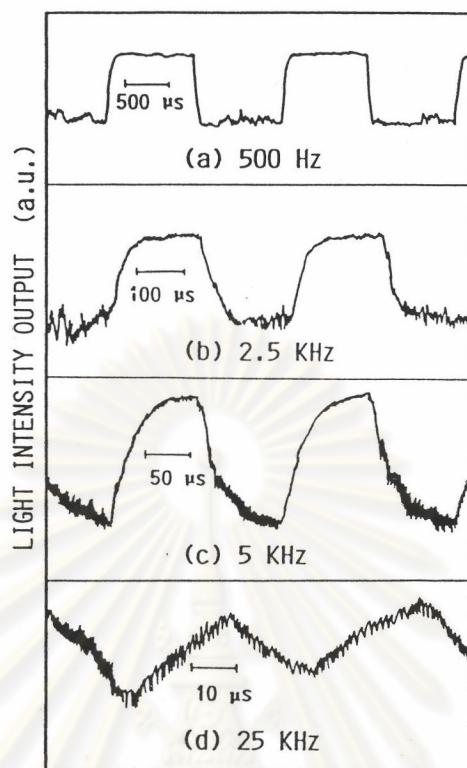
Figure 3.36 Typical light output waveform response to an input square-wave current pulse for a yellow a-SiN:H TFLED.
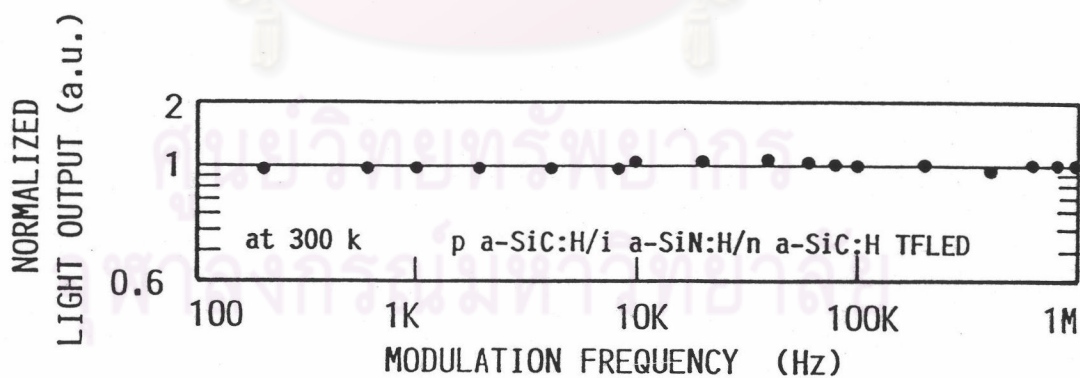

Figure 3.37 Dependence of the EL intensity on the modulation frequency in the range of 100 Hz to 1 MHz for a yellow a-SiN:H TFLED.

3.6 Fabrication of a-SiN:H TFLED Display

It was described in section 3.5 that the a-SiN:H TFLED has been developed for the first time. The operation voltage was as low as 5-10 V, which is much lower than the case of intrinsic EL type displays. The color of the a-SiN:H TFLED can be changed from red to yellow by varying the optical energy gap of the i-a-SiN:H layer. The brightness was about 0.7-0.8 cd/cm^2. The pattern of the emission described so far was simple circle and rectangle with the area of 0.033-0.15 cm^2. In order to use the a-SiN:H TFLED as a display, the TFLED has to display the emission with any desired pattern of the picture.

In this section, the fabrication process of the a-SiN:H TFLED display will be described. The emitting patterns of the amorphous TFLED display can be classified into two types as follows:

1. Fixed emitting pattern,

and   2. Movable emitting pattern

In this chapter, the fabrication technology of the a-SiN:H TFLED with fixed emitting patterns is described. The designs and fabrication technologies of the movable emitting pattern will be described in chapter 6.

3.6.1 a-SiN:H TFLED with Fixed Emitting Pattern

The a-SiN:H TFLED that emits the light with a desired fixed pattern was fabricated. The emitting pattern is the pattern of the current flowing across the sample. The actual designs are shown in Figures 3.38 (a) - (c).

In Fig. 3.38 (a), the emitting pattern was determined by the pattern of the Al electrode. First, the ITO transparent front electrode was evaporated onto the whole area of the glass substrate. Second, the amorphous p-i-n layers were deposited onto the whole area of the glass substrate. The optimal thicknesses of the p-i-n layers were 150 Å, 500 Å and 500 Å, respectively. Finally the Al rear electrodes with specified pattern are deposited onto the amorphous p-i-n layers. The emission was observed at
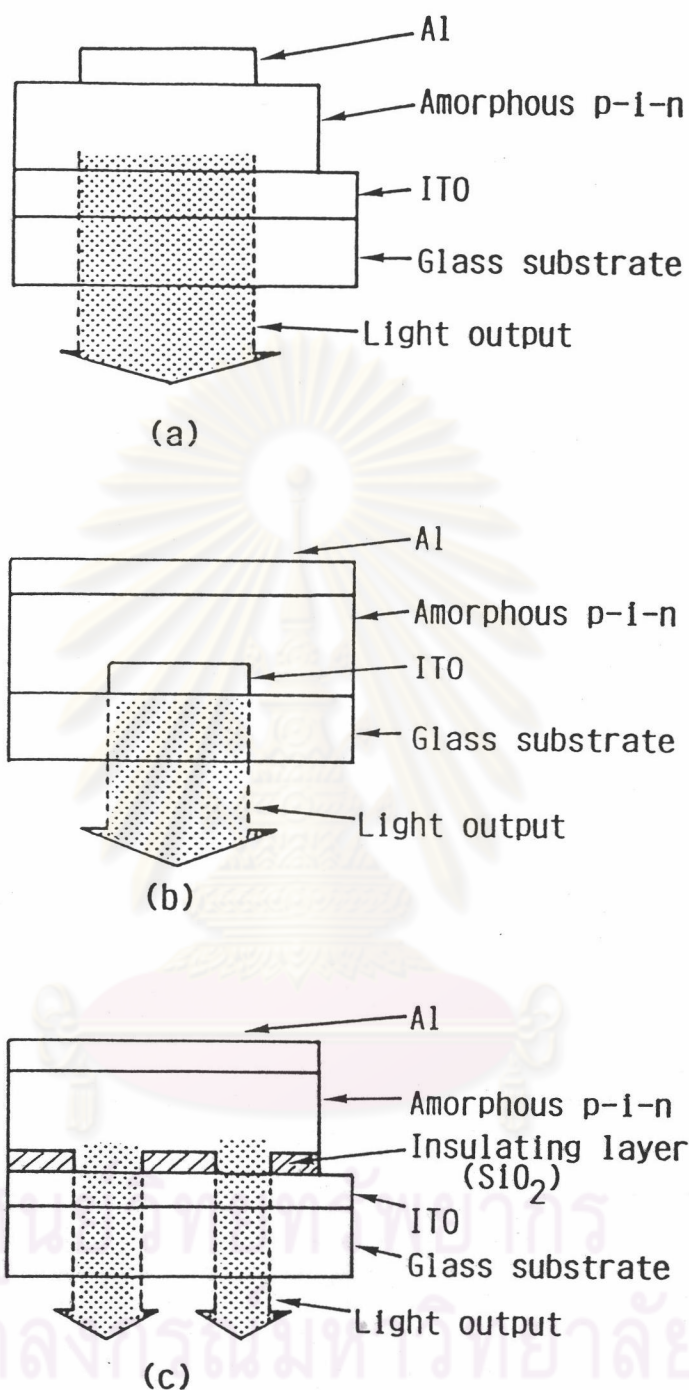
Figure 3.38 Design rules for fixed emitting patterns of a-SiN:H TFLED.

(a) The emitting pattern is determined by the pattern of the Al electrode.

(b) The emitting pattern is determined by the pattern of the ITO electrode.

(c) The emitting pattern is determined by the pattern of the insulating layer inserted in the device.

the crossing area of the front and rear electrodes. This pattern of the Al electrode was made through the stainless steel mask.

In Fig. 3.38 (b), the emitting pattern was determined by the pattern of the ITO electrode. Firstly, the ITO transparent front electrode with the specified pattern was evaporated onto the glass substrate. Next the amorphous p-i-n layers and the Al electrode, respectively, were deposited onto the whole area of the glass substrate. The emission was observed at the crossing area of the front and rear electrodes. The ITO front electrode pattern was made through a stainless steel mask or by etching technique. The acid for etching ITO was $HCl + FeCl_2 +$ water.

In Fig.3.38 (c), the emitting pattern was determined by the pattern of the insulating layer inserted into the device. One of the advantages of this technique was that complicated and isolated patterns could be realized. The materials of the insulating layer were for example, SiO_2, a-SiC:H, a-SiN:H, Y_2O_3. The photolithography and lift-off techniques were powerful in this technique. The emitting pattern was observed at the area where the insulating layer does not exist.

In this work, we succeeded in the fabrication of the amorphous TFLEDs by the above mentioned.

3.6.1.1 Determination of Fixed Emitting Pattern by Al Electrodes

Figure 3.39 shows the pictures of metal masks for the evaporation of Al rear electrodes.

Figure 3.40 shows the pictures of the a-SiN:H TFLEDs before emitting the light. The patterns of circles and rectangular were due to the Al electrodes deposited through metal masks.

Figure 3.41 shows the pictures of the actual emissions of circle red, yellow and white-blue a-SiN:H TFLEDs. The diameter of the circle is 2 mm. The optical energy gaps of the i-a-SiN:H TFLEDs are 2.50, 2.80 and 3.60 eV, respectively. The injection current density in the pictures is 150 mA/cm^2.
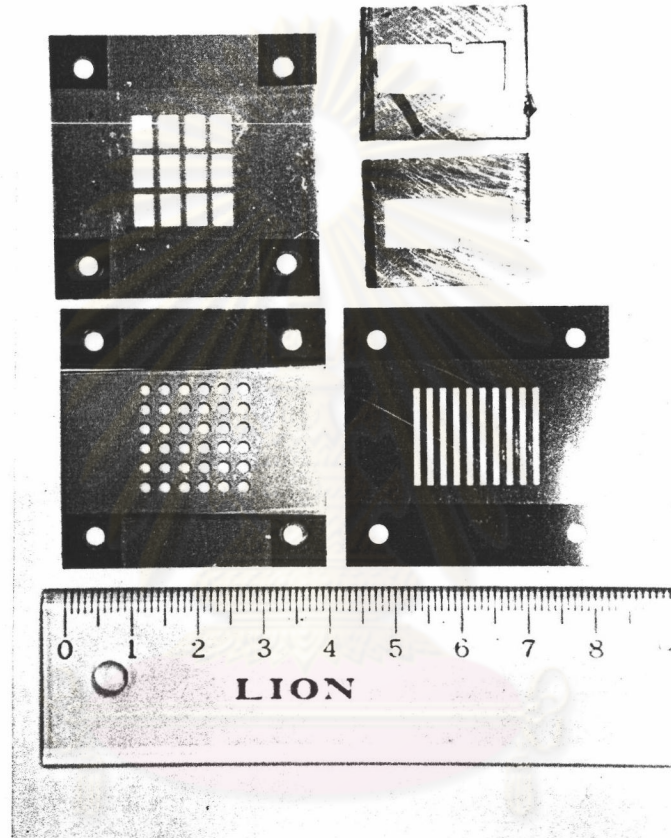
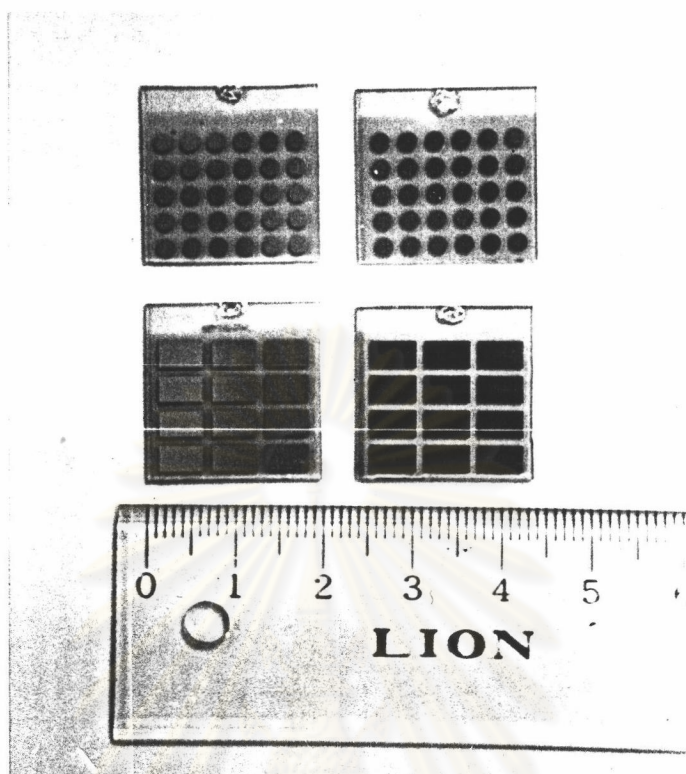Figure 3.39 Photographs of metal masks for the evaporation of Al rear electrodes.

Figure 3.40 Photographs of the a-SiN:H TFLEDs before emitting the light.
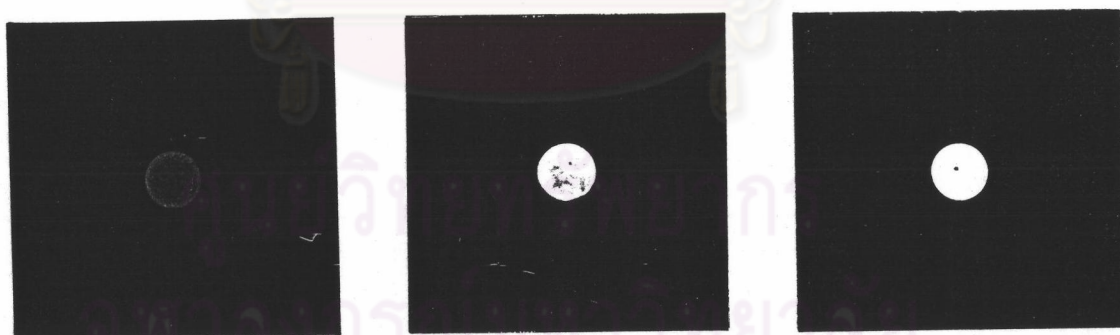

Figure 3.41 Photographs of the actual emissions of circle red, yellow and white-blue
a-SiN:H TFLEDs. The diameter of the circle is 2 mm. The optical
energy gaps of the i-a-SiN:H TFLEDs are 2.50, 2.80 and 3.60 eV,
respectively. The injection current density is 150 mA/cm².

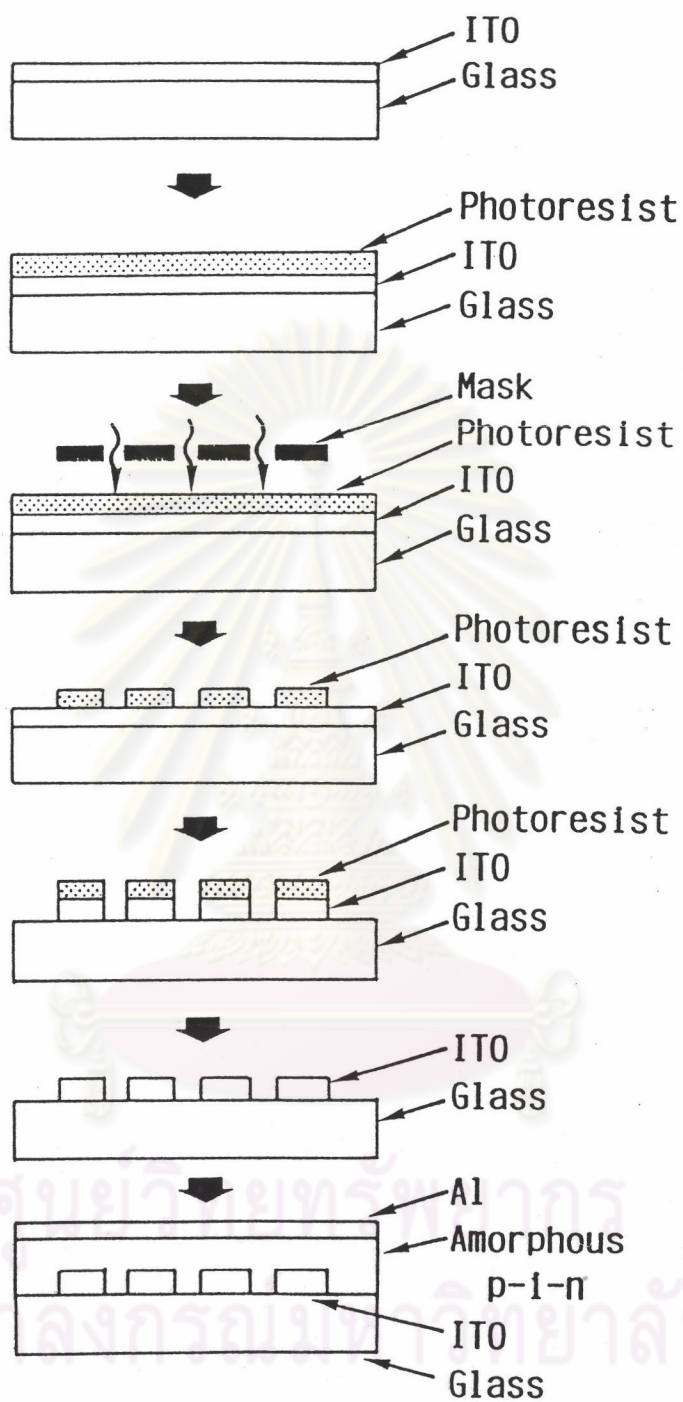Figure 3.42 Fabrication process of the ITO electrode with a desired pattern for using in a visible-light amorphous TFLED.
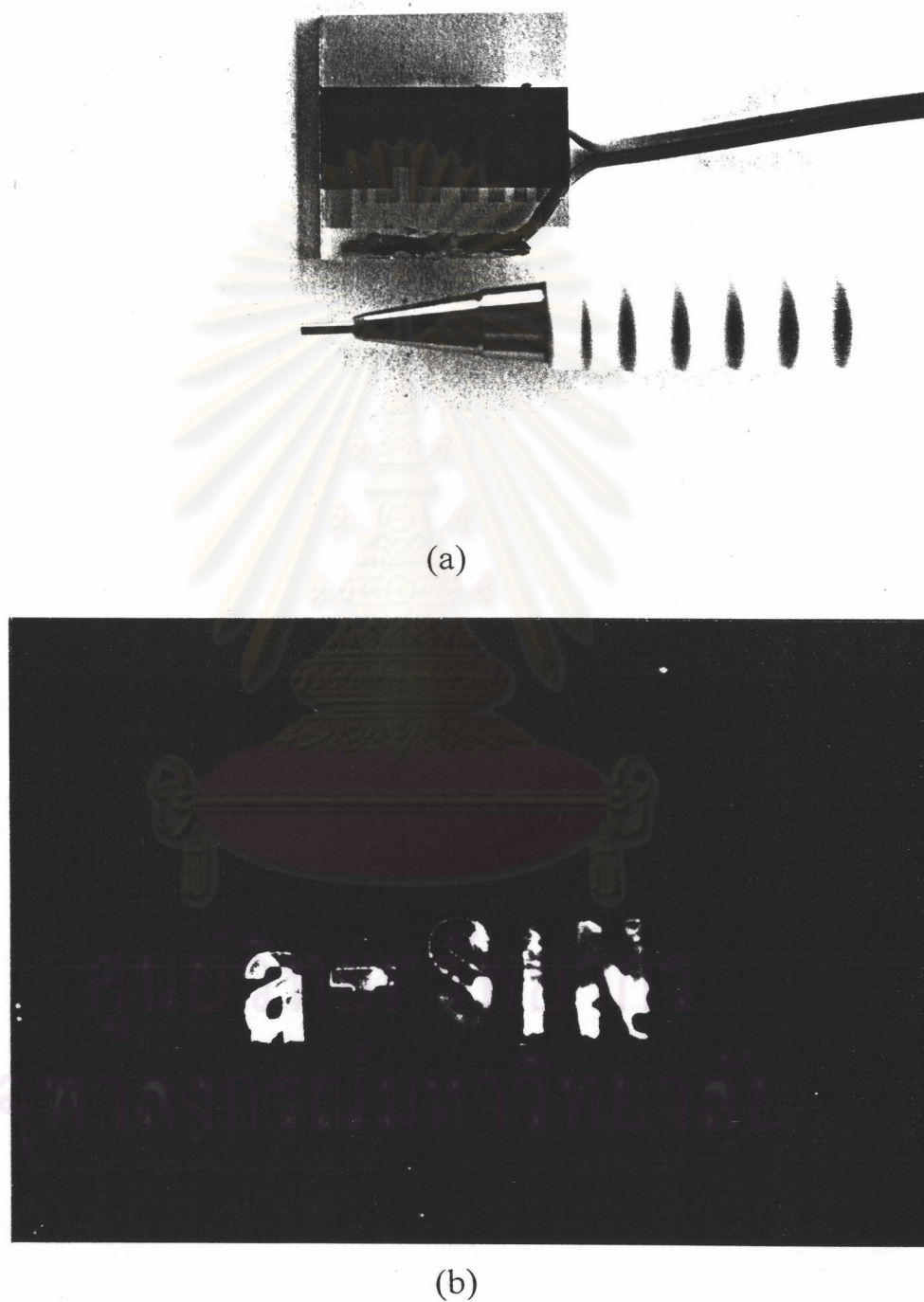
(a)

(b)

Figure 3.43 Photograph of the actual emission from the a-SiN:H TFLED, (a) before emit the light and (b) during emitting white-blue color light. The emitting pattern of the alphabet "a-SIN" was determined by the ITO electrodes. The height of emitting pattern is 6 mm.

3.6.1.2 Determination of Fixed Emitting Pattern by ITO Electrodes

Figure 3.42 shows the fabrication processes of a desired ITO pattern of a-SiN:H TFLED. The ITO transparent film was evaporated onto the whole area of the glass substrate and the pattern of the ITO was determined by using photolithography and etching techniques.

Figure 3.43 shows the pictures of the actual emission from the a-SiN:H TFLED (a) before emit the light and (b) during emitting white-blue color light. The emitting pattern of the alphabet "a-SIN" was performed by the ITO electrodes. The height of emission pattern is 6 mm.

3.7 Summary

A series of systematic investigations has been done on the structural and optical properties of a-SiN:H characterized by IR absorption, ESR, optical absorption and photoluminescent (PL) measurements. It has been shown that the undoped a-SiN:H possessing a wide range of optical energy gap from 1.8 eV to 3.1 eV can be prepared by adjusting the ratio of the nitrogen source gas (ammonia gas) to the silane gas. The PL emission color changes from red to green along with the increase in the optical energy gap. The PL peak energy is somehow smaller than the optical energy and also shows a strong dependence on the excitation photon energy when the excitation energy is less than the optical energy gap. These results suggests that the radiative recombination process involves localized states which are widely distributed within the gap. This point gives an important insight in understanding the basic properties the a-SiN:H TFLEDs.

The quality of the a-SiN:H prepared in this work was good enough to be used as the luminescent active layer in the visible-light thin film light emitting diode (TFLED). A visible-light TFLED with a-SiN:H active i-layer has been developed for the first time. The device structure is glass/ITO/p-a-SiC:H/i-a-SiN:H/n-a-SiN.H/Al. The emission color can be varied from red to yellow by adjusting the optical energy gap of the i-a-SiN:H layer. In order to obtain a visible light emission, the optical energy gap of the i-layer has to be larger than 2.5 eV, while the optical energy gaps of

the p- and n-layer are kept constant around 2.0 eV to ensure the valency controllability.

A systematic study on the carrier injection mechanism and EL property in this kind of heterojunction TFLEDs has been done. The result has revealed that the carrier injection mechanism in the a-SiN:H TFLED is based upon the tunneling injections of holes and electrons from the small gap p- and n-layers into the wide gap i-layer through the notch barriers at the p/i and i/n heterointerfaces. Based upon this analysis, a simple optimization of the thickness of the i-a-SiN:H layer has been done. At the present stage the brightness obtained so far is about 0.7-0.8 cd/m^2. The external luminescence efficiency is estimated to be the order of 10^{-3} %.

An investigation on the frequency modulation characteristic revealed that the brightness of the a-SiN:H TFLED does not decrease even the frequency of the input pulse current is as high as 1 MHz. This performance of the a-SiN:H TFLED satisfies the requirement for the utilization as a display which is generally operated in a pulse current scanning mode with the frequency of several kHz.

Finally some unique designs and fabrication of a-SiN:H TFLED as flat panel displays have been proposed and demonstrated. The yellowish orange and white-blue a-SiN:H TFLED displays with emission area of several cm^2 have been demonstrated.

References

1. Hirose, M. Amorphous semiconductor technologies & devices. In Y. Hamakawa (ed.), <u>Japan annual reviews in electronics, computers & telecommunications,</u> 6 pp. 173. Ohmsha, Ltd. and North-Holland, Japan, 1983.

2. Anderson, D.A. and Spear, W.E.. Electrical and optical properties of amorphous silicon carbide, nitride and germanium carbide prepared by the glow discharge technique. <u>Phil. Mag.</u> 35 (January 1977) : 1-16.

3. Kurata, H., Miyamoto, H., Hirose, M. and Osaka, Y. <u>Jpn. J. Appl. Phys.</u> 21 Suppl. 21-2 (1982) : 205.

4. Nogichi, T., Usui, S., Sawada, A., Kanoh, Y., and Kukichi,M. <u>Jpn. J. Appl. Phys.</u> 21 (1982) : L485.

5. Irabaki, N., and Fritzsche, H. Properties of amorphous semiconducting a-Si:H/ a-SiN:H multilayer films and of a-SiN$_x$:H alloys. <u>Phys. Rev. B.</u> 30 (1984) : 5791-5799.

6. Morimoto, A., Tsujimmura, Y., Kumeda, M., and Shimizu, T. <u>Jpn. J. Appl. Phys.</u> 24 (1985) : L394.

7. Osenbach, J.W. and Knolle, W.R. <u>J. Appl. Phys.</u> 60 (1986) : 1408.

8. Robertson, J. <u>Appl. Phys. Lett.</u> 44 (1984) : 415.

9. Narikawa, S., Kojima, Y., and Ehara, S. <u>Jpn. J. Appl. Phys.</u> 24 (1985) : L861.

10. Spear, W.E., Dunnett, B., and LeComber, P.G. Substitution and interstitial doping of amorphous silicon nitride. <u>Mat. Res. Soc. Symp. Proc.</u> 95 (1987) : 39-49.

11. Dunnett, B., Jones, D.I., and Stewart, A.D. <u>Philos. Mag.</u> 53 (1986) : 159

12. Kurata, H., Hirose, M., and Osaka, Y. Wide optical-gap, photoconductive a-Si$_x$N$_{1-x}$:H. <u>Jpn. J. Appl. Phys.</u> 20 (November 1981) : L811-L813.

13. Kruangam, D., Boonkosum, W., Siamchai, P., and Panyakeow, S. Amorphous visible-light thin film LED having a-SiN:H as a luminescent layer. Extended Abstracts of the 1992 International Conference on Solid State Devices and Materials. Tsukuba Center Building. Tsukuba. Japan. (August 26-28. 1992) : 563-565.

14. Boonkosum, W., Kruangam, D., and Panyakeow, S. Amorphous visible-light thin film light-emitting diode having a-SiN:H as a luminescent layer. Jpn. J. Appl. Phys. 32 No. 4 (April 1993) : 1534-1538.

15. Boonkosum, W., Kruangam, D., and Panyakeow, S. Visible-light amorphous silicon-nitride thin film light emitting diode. Mat. Res. Soc. Symp. Proc. 297 (1993) : 1005-1010.

16. Boonkosum, W., Kruangam, D., and Panyakeow, S. Novel flat-panel display made of amorphous SiN:H/SiC:H thin film LED. International Symposium of Physical Concepts and Materials for Novel Optoelectronic Device Applications II. Trieste. Italy. SPIE 1985. (May 24-27. 1993) : 40-51.

17. Kruangam, D., Boonkosum, W., and Panyakeow, S. Visible thin film light emitting diode using a-SiN:H/a-SiC:H heterojunctions. J. of Non-Crys. Sol. 164-166 (1993) : 809-812.

18. Landford, W.A., and Rond, M.J. J. Appl. Phys. 49 (1978) : 2473.

19. Shimizu, T., Oozora, S., Morimoto, A., Kumeda, M., and Ishii, U. Solar Energy Mater. 8 (november 1982) : 311-317.

20. Ishii, N., Morimoto, A., Kumeda, M., and Shimizu, T. Proc. Int. Conf. Phys. Semiconductors. San Francisco. Springer-Verlag, New York. (1984) : 921.

21. Street, R.A., Knights, J.C., and Biegelsen, D.K. Luminescence studies of plasma-deposited hydrogenated silicon. Phys. Rev. B 18 (1978) : 1880-1891.

22. Pankove, J.I. (ed.). Hydrogenated amorphous silicon, semiconductors and semimetals. 21. A, B, C, and D (1984).

23. Taylor, P.C. and Bisshop, S.G. Optical effects in amorphous semiconductors. Amer. Inst. of Physics Conf. Proc. 120 (1984).

24. Street, R.A., Biegelsen, D.K., and Zesch, J. Spin-dependtent recombination at dangling bonds in a-Si:H. Phys. Rev. B 25 (1982) : 4334-4337.

25. Street, R.A. Phys. Rev. Lett. 49 (1982) : 1187-1190.

26. Bauer, G.H. and Bilger, G. Properties of plasma-produced amorphous silicon governed by parameters of the production, transport and deposition of Si and SiN$_x$. Thin Film Solids 83 (1981) : 223-229.

27. Engeman, D. and Fischer, R. Radiative and non-radiative recombination in amorphous silicon. AIP Conf. Proc. 31 (1976) : 37-43.

28. Bhat, P.K., Searle, T.M., Austin, I.G., and Gibson, R.A. Low energy excitation of photoluminescence in a-Si:H temperature and intensity effects. Sol. Stat. Commun. 45 (June 1983) : 481-484.

29. Chen, W.C., Feldman, B.J., Bajaj, J., Tong, F.M, and Wong, G.K. Thermalization gap, excitation photoluminescence and optical absorption in amorphous silicon-hydrogenated alloy. Sol. Stat. Commun. 38 (1981) : 357-360.

30. Nakazawa, E., Munekata, H., and Kukimoto, H. Picosecond time-resolved luminescence of hydrogenated amorphous silicon-carbide. Sol. Stat. Commun. 45 (October 1983) : 925-927.

31. Kurata, S., Czaja, W., and Kinmond, S. Sol. Stat. Commun. 32 (1979) : 879.

32. Nashashibi, T.S., Austin, I.G., and Searle, T.M. Photoluminescence in doped and undoped amorphous silicon. Proc. 7th Int. Conf. Amorphous and Liquid Semiconductors (1977) : 392-396.

33. Street, R.A., Tsang, C., and Knights, J.C. Photoluminescence in a-Si:H. Proc. Int. Conf. Phys. Semicond. Edingbergh. (1978) : 1139-1142.

34. Paesler, M.A. and Paul, W. Phil. Mag. B 41 (1980) : 393.

35. Kruangam, D.   Amorphous and microcrystalline silicon-carbide alloy light emitting diodes. In J. Kanicki (ed.) , <u>Physics and properties, in amorphous and microcrystalline semiconductor devices: optoelectronic devices</u>, pp. 165-240. Artech House : Boston, London, 1991.
36. Pilkuhn, M.H.   Handbook of Semiconductors. In Cyril Hilsum (ed.) , <u>Light emitting diodes</u>, pp. 607-609. North-Holland, 1981.